Technische Universität München

Max-Planck-Institut für Biochemie
Abteilung Membran- und Neurophysik

RIKEN Brain Science Institute
Laboratory for Neuronal Circuit Dynamics

Optical recording of neuronal circuit dynamics

Alexander M. Wolf

Vollständiger Abdruck der von der Fakultät für Physik der Technischen Universität München zur Erlangung des akademischen Grades eines

Doktors der Naturwissenschaften

genehmigten Dissertation.

Vorsitzender: Univ.-Prof. Dr. M. Rief

Prüfer der Dissertation:

1. Hon.-Prof. Dr. P. Fromherz
2. Univ.-Prof. Dr. J. L. van Hemmen

Die Dissertation wurde am 17.2.2004 bei der Technischen Universität München eingereicht und durch die Fakultät für Physik am 7.10.2004 angenommen.

Summary

This work deals with the optical recording of cerebellar circuit dynamics from acute brain slices of the cerebellar surface. This preparation preserves the functional connectivity of the cerebellar cortex. It was used to investigate the function of Kv3 potassium channels in the cerebellar granule cell axon. Double knockout mice lacking both Kv3.1 and Kv3.3 potassium channels display severe motor deficits, while mice lacking only Kv3.1 or Kv3.3 do not. Since granule cells express both Kv3.1 and Kv3.3, they were the candidate neuron type to be involved. Optical recording of action potentials from parallel fibers revealed a broadening of the action potential in mice lacking Kv3.1 and Kv3.3 and in mice lacking Kv3.1 and one allele of Kv3.3. The transmission of high-frequency trains of action potentials was impaired in double knockout mice. Parallel fiber conduction velocity was increased in mice lacking 3 or 4 Kv3 alleles. Paired-pulse facilitation at the parallel fiber – Purkinje cell was reduced in a gene-dose dependent manner and the induction of metabotropic glutamate receptor-mediated potentials facilitated in double knockout mice. Most of the changes were expected from the previously known function of Kv3 channels in other cell types, but some changes were unexpected, such as an increase in conduction velocity. To understand and explain the changes, a compartmental model of the granule cell axon was constructed. The model explained many mechanisms underlying the alterations observed in the experiment, among them why and how parallel fiber conduction velocity was dependent on the density or the expression of Kv3.1 and Kv3.3 potassium channels. The results demonstrate the power of optical imaging methods in investigating cerebellar cortical function and the importance of Kv3 potassium channels in regulating the dynamics of synaptic transmission at the parallel fiber-Purkinje cell synapse.

Zusammenfassung

Die Arbeit untersucht die Auswirkung der spannungsabhängigen Kaliumkanäle Kv3.1 und Kv3.3 auf die synaptische Transmission in den Axonen der Körnerzellen des Kleinhirns, den Parallelfasern. Mit spannungssensitiven Fluoreszenzfarbstoffen und schnellen CCD-Kameras wurde die Form und Ausbreitungsgeschwindigkeit der Aktionspotentiale in akuten Schnitten des Kleinhirns gemessen. Gentechnischer Knockout von Kv3.1 und Kv3.3 verbreitert das Aktionspotential, erhöht dessen Ausbreitungsgeschwindigkeit und vermindert die Fähigkeit der Axone, Aktionspotentiale mit hoher Frequenz zu übertragen. Elektrophysiologische Messungen an den Purkinjezellen demonstrierten veränderte Kurzzeitplastizität und früheres Auslösen postsynaptischer Potentiale durch metabotrope Glutamatrezeptoren in Purkinjezellen von Kv3.1/Kv3.3 Knockoutmäusen. Ein biophysikalisches Modell des Axons erklärt die Mechanismen, durch die die Kaliumkanäle Kv3.1 und Kv3.3 die Eigenschaften der Parallelfasern beeinflussen.

Table of Contents

1. Introduction

The human brain is the most complex structure known so far. Information processing occurs distributed to billions of neurons in parallel. To understand its processing of information, it is necessary to record activity from many locations in parallel. Optical recording is one technique to achieve this, and in comparison to other environment-sensitive fluorescent dyes or intrinsic signals, voltage-sensitive dyes offer the highest temporal resolution and the ability measure membrane potential, presumably the most important measure of neuronal activity.

The cerebellum is a structure of remarkably simple cellular connectivity (Eccles et. al., 1967). The neuronal components of the cerebellar cortex are arranged in a geometrical pattern which is essentially a laminated array of a rectangular lattice (Braitenberg and Atwood, 1958). This simple neuronal arrangement that is conserved across a wide range of species has led to the assumption that the cerebellum can be regarded as a “neuronal machinery” designed to process information in a unique and essential manner. Many postulates have been made based on the anatomical connectivity of the cerebellar cortex. Despite the relative simple organization that is known for close to 100 years, surprisingly little is known about how the cerebellum performs it function. The cerebellum has been found to be involved in the fine control of movement and timing and the parallel fibers, one of the most striking features of the cerebellar cortex, have been postulated to function as a delay line (Braitenberg and Atwood, 1958). Plasticity of connections between parallel fibers is related to motor learning (Ito, 2000).

This dissertation deals with the optical recording of neuronal circuit dynamics in acute slices of the cerebellar cortex using voltage sensitive dyes. Although this technology of optical recording from brain slices was applied to several brain regions during the course of this dissertation (Iwasato et al., 2000; Tsutsui et al., 2001), the main work was done using a slice preparation of the surface of the cerebellar cortex of the mouse. Some of the results of this work have been published (Matsukawa et al., 2003).

The dissertation starts with a description of the optical recording methodology. Technical aspects such as light source, optics and detection of fluorescence using fast CCD cameras are outlined.

To familiarize the reader with the cerebellum, the anatomy and functional organization of the cerebellar cortex are briefly recapitulated. The superficial slice preparation allowed for successful optical imaging of a variety of phenomena underlying cerebellar function, such as the spatio-temporal dynamics of action potential propagation and synaptic transmission. Recording these phenomena at previously unattained spatial and temporal resolution with high signal-to-noise ratio gave new insights into several phenomena relevant to cerebellar information processing

Optical recording of action potential propagation in the cerebellar cortex was used to investigate the dynamics of synaptic transmission in fast voltage-gated Kv3.1/Kv3.3 potassium channel knockout mice. Recording the voltage-sensitive dye signals corresponding to action potentials propagating along parallel fibers, it was found that lack of Kv3.1 and Kv3.3 causes the action potential to broaden. Furthermore, mice lacking alleles for the Kv3.1 or Kv3.3 genes showed increased parallel fiber conduction velocity and

impairment in conducting trains of action potentials above 100 Hz. To test whether the changes in presynaptic action potential shape cause the expected changes in short-term plasticity, whole-cell patch-clamp recording was performed and confirmed the expected reduction of paired-pulse facilitation at the parallel fiber – Purkinje cell synapse. Lack of Kv3.1 and Kv3.3 channels was also found to greatly decrease the number of stimuli required to induce metabotropic glutamate receptor mediated excitatory postsynaptic currents. These changes should have a strong effect on cerebellar functions such as motor learning and might be the cause for some of the phenotypic alterations in these mice.

To understand and explain some of the changes found in parallel fiber action potential shape and especially conduction velocity, a compartmental model of the granule cell axon (the parallel fiber) was constructed using the NEURON simulation environment. Activity- and potassium channel dependent changes are investigated in detail and compared with the experimental findings. The parallel fiber model explained many mechanisms underlying the alterations observed in the experiment, among them why and how parallel fiber conduction velocity was dependent on both activity and on the expression of Kv3.1 and Kv3.3 potassium channels.

Several phenomena relevant to cerebellar cortical function have been recorded at previously unattained spatial and temporal resolution in this work. The automated analysis of fluorescence time series resulted in a wealth of data about many important aspects of parallel fiber dynamics. This work demonstrates the power of optical recording methods to answer questions that can not be addressed with other methods.

2. Optical recording of membrane potential

Understanding the spatio-temporal features of the information processing occurring in any complex neural structure requires the monitoring and analysis of the activity in populations of neurons. Classical intracellular and extracellular electrophysiological techniques, including single cell and extracellular field recordings, have provided important insights into the function of neural circuits in many systems. Even with the significant insights gained using single and multiple electrode recordings, there remain limitations. For example, it is difficult to achieve high-density maps of neural activity using extracellular recording techniques. Monitoring changes in membrane potential in small cells or fine processes, or recording from embryonic or developing neurons is also extremely problematic. Therefore, complementary techniques that permit the monitoring of the spatial-temporal activity in neuronal populations are of continued interest. The ideal technique would be non-invasive and would have a spatial resolution at the single cell level or even at the level of processes of single cells. The ideal temporal resolution would be in the tens of microseconds range, sufficient to study action potential and synaptic potentials. This is not achieved with currently available techniques. Practically, however, what is required is a spatial and temporal resolution sufficient to answer the question addressed and there are many open questions in neuroscience that can only be answered using optical imaging techniques.

2.1 Voltage-sensitive dyes

The use of voltage-sensitive dyes coupled with optical recording techniques to monitor electrical activity has been a promising approach for a long time. The pioneering work of Cohen, Salzberg, Grinvald and their co-workers laid the groundwork for what has become a rapidly growing and maturing field (Cohen, 1993). What was and remains attractive about voltage-sensitive dyes and optical imaging is that they come close to the ideal of non-invasive recording of activity with high spatial and temporal resolution. In general, there are two broad classes of voltage-sensitive dyes, “slow” and “fast”. Most slow dyes use a potential-dependent distribution mechanism and have equilibration time constants of 1-20 seconds. Therefore, they are of limited utility for information processing questions.

The “fast” voltage-sensitive dyes are fluorescent organic molecules that bind to the cell membrane. Several classes of fast voltage-sensitive dyes exist, amongst them the styryl (aminostyryl-pyridinium) dyes. When bound to a membrane, the positively charged pyridinium ring is oriented towards the extracellular space with the long axis of molecule perpendicular to the membrane surface. The exact mechanism of the voltage sensitivity of these dyes has not been elucidated yet, but it is due to both molecular motion and electron motion in reaction to a change in electric field across the membrane, leading to a modulation of fluorescence properties of the dye molecule. Styryl dyes have been shown to exhibit response times of less than 2 microseconds (Loew et. al., 1985). The styryl dye di-4-ANEPPS

(dibutylaminonaphtylethylenepyridiniumpropylsulfonate, Fig. 2.1) has been found to exhibit favorable properties in a variety of preparations (Ebner and Chen, 1995) and was used exclusively in this work. Its voltage sensitivity is due to a blue shift of the absorption spectrum, a weaker blue shift of the emission spectrum, a spectral broadening of fluorescence and a drop in the fluorescence quantum yield (Fromherz and Lambacher, 1991). Di-4-ANEPPS was purchased from Molecular Probes.

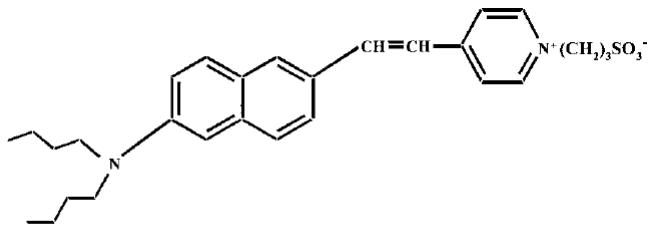

Fig. 2.1: Chemical Structure of di-4-ANEPPS.

Brain slices were stained with the voltage sensitive dye at a concentration of 5µM for 30 minutes in oxygenated ACSF. The dye is dissolved in a stock solution of ethanol & DMSO mixed at a ratio of 2:1. Immediately prior to staining, the stock solution is diluted in oxygenated ACSF at a ratio of 200:1 to yield a final concentration of 5µM di-4-ANEPPS. At this concentration, neither ethanol nor DMSO (Jourdon et al., 1986; Nakahiro et al., 1992; Winckler et al., 1999; Lu & Mattson, 2001) have any toxic effects.

This staining procedure will stain membranes exposed to the extracellular solution up to a depth of about 500-600 microns into the brain slice via diffusion of the dye either in the extracellular solution or in the (plasma) membrane (see also Kleinfeld & Delaney (1996), Fig. 2). A reduction

in dye concentration appeared at 200-300 µm depth. Brain slices of a thickness of 500 µm (stained from both sides) will therefore be stained more or less homogeneous. Since di-4-ANEPPS is a lipophilic dye and there was little decay of the optical signal size during the experiment, it can be assumed that the dye stayed in the external leaflet of the plasma membrane for the duration of the experiments (Tsau et al., 1996). Staining of intracellular organelles can also assumed to be weak or absent. Cell-type- and preparation-dependent staining efficiencies have been reported for different voltage-sensitive dyes (Ebner and Chen, 1995). The optical signals we obtained were as one would expect from the distribution of neuronal membranes in the cerebellar cortex, and di-4-ANEPPS seemed to stain every cell type in our hands.

2.2 Optical recording system

A relatively simple epifluorescence setup (shown in Fig. 2.2) was used to record optical signals from *in vitro* brain slices. The optics consisted of 1.6X objective, dichroic mirror (575 nm), longpass filter (590 nm) and inverted 1.6X objective mounted above the slice. Fluorescence was excited with an ultra stable (less than 0.1% intensity fluctuation) green laser, a frequency-doubled Nd:YVO laser (Verdi, Coherent) of 532 nm wavelength (Fig.2.3). Since the laser stability is best at near maximum power (10 Watt), the intensity was reduced by reflecting the laser with 2 glass plates and passing it through several neutral density filters. An electromechanical shutter was inserted into the beam path to control illumination. The beam is fed into a steel-encased

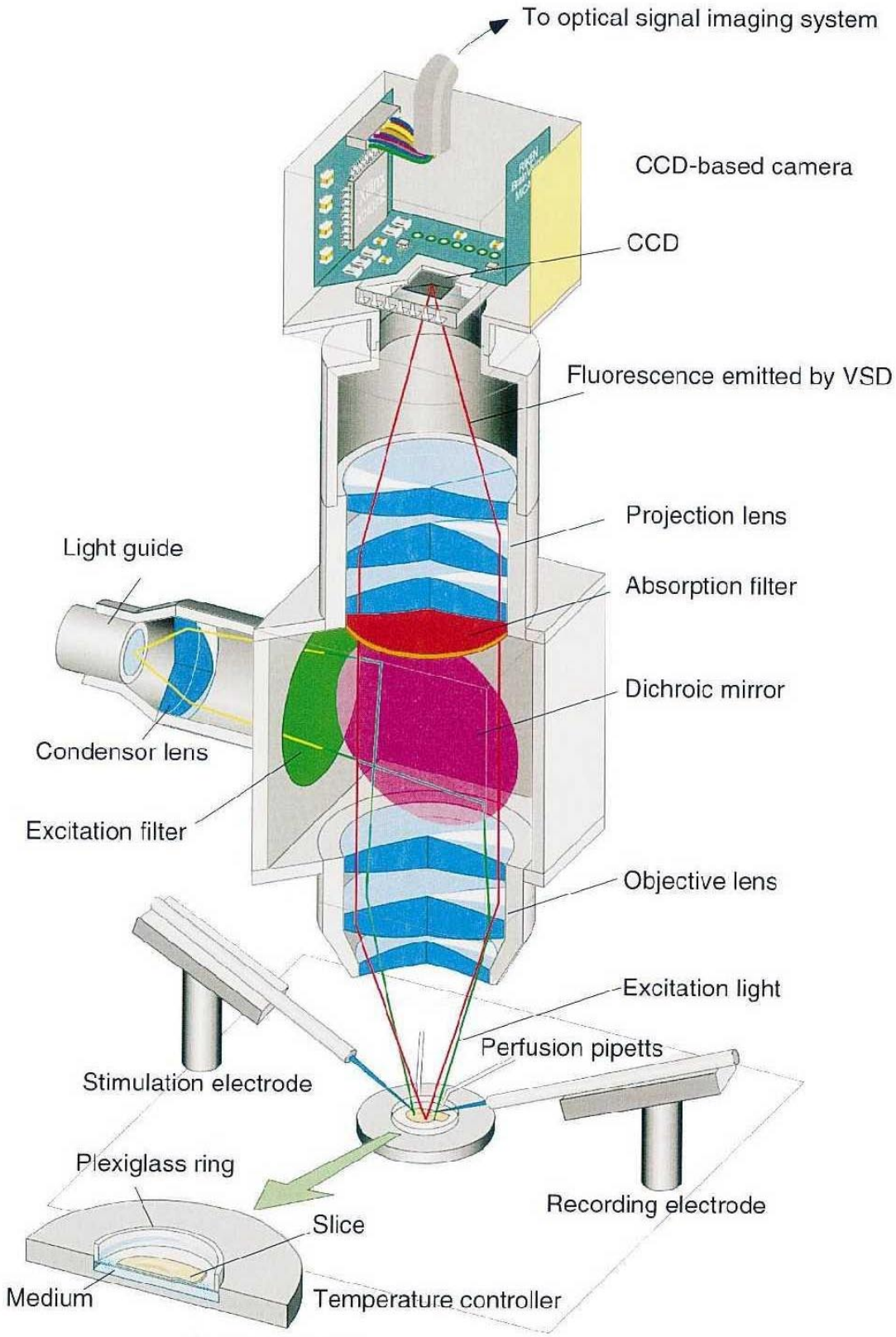

Fig. 2.2 Schematic setup (taken from Tominaga et al., 2000) with illumination (green lines) and emission by the voltage-sensitive dye (VSD, red lines).

multimode glass fiber with 2 millimeter core diameter (QMMJ-55-IRVIS-940/1000-5AS-5, Linos Photonics) using a high power laser coupler (HPUC-25-532-M-15PX-12, Linos Photonics).

Optionally the laser can be diverted into an electro-optic modulator followed by a polarizing beamsplitter. The electro-optic crystal rotates the polarization of the laser beam depending on the voltage applied. In connection with the polarizing beamsplitter deflecting the horizontally polarized component, this allows extremely fast switching of the laser

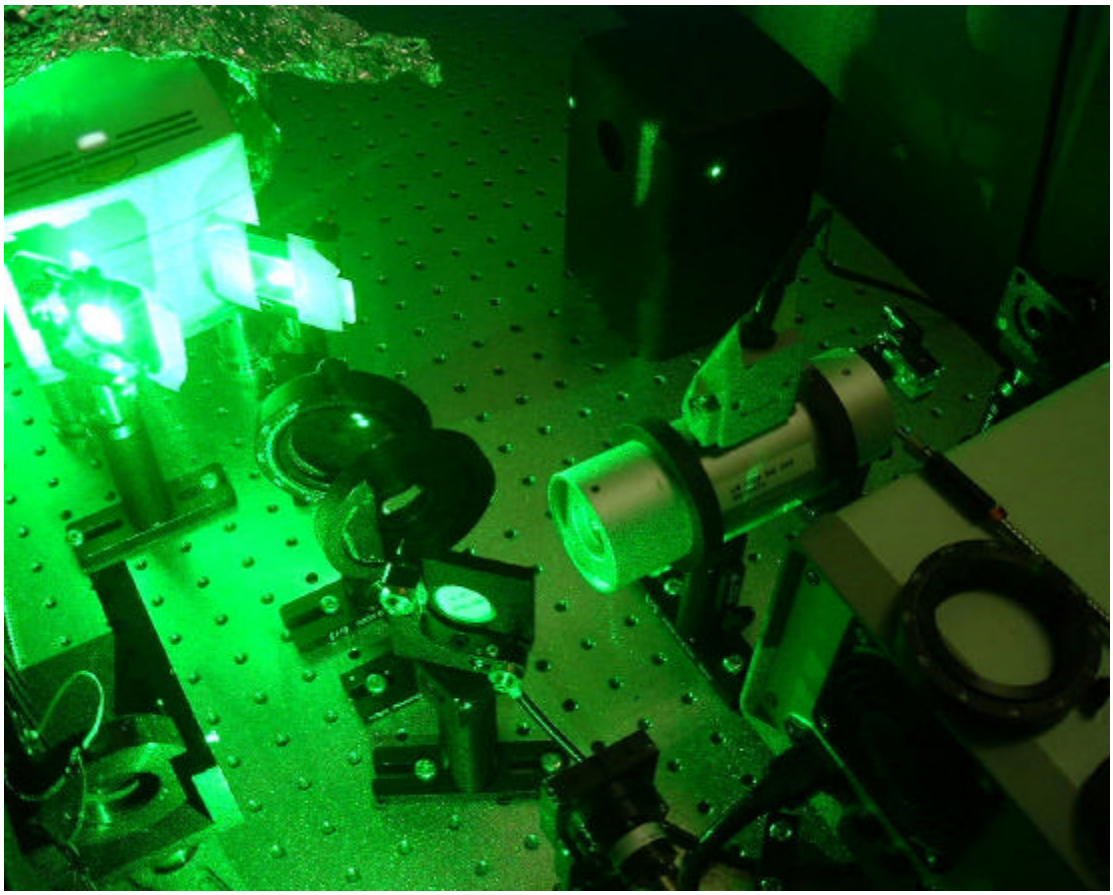

Fig. 2.3: The laser excitation part of the setup, consisting of the laser (top), followed by 2 glass plates and a neutral density filter to reduce intensity, shutter, a flip mirror to the optional electro-optic switch and the laser coupler.

intensity. This can be used to increase the time resolution beyond the camera speed using stroboscopic illumination (See Annex 1).

The excitation light passes through the optical fiber to the imaging setup (Fig. 2.4). After emerging from the fiber, the light is parallelized using a laser collimator (HPUCO-25-532-M-25BQ, Linos Photonics), a specialized condensor lens positioned its focal length away from the fiber end. Coupler, collimator and fiber use the SMA fiber connector standard. The excitation light

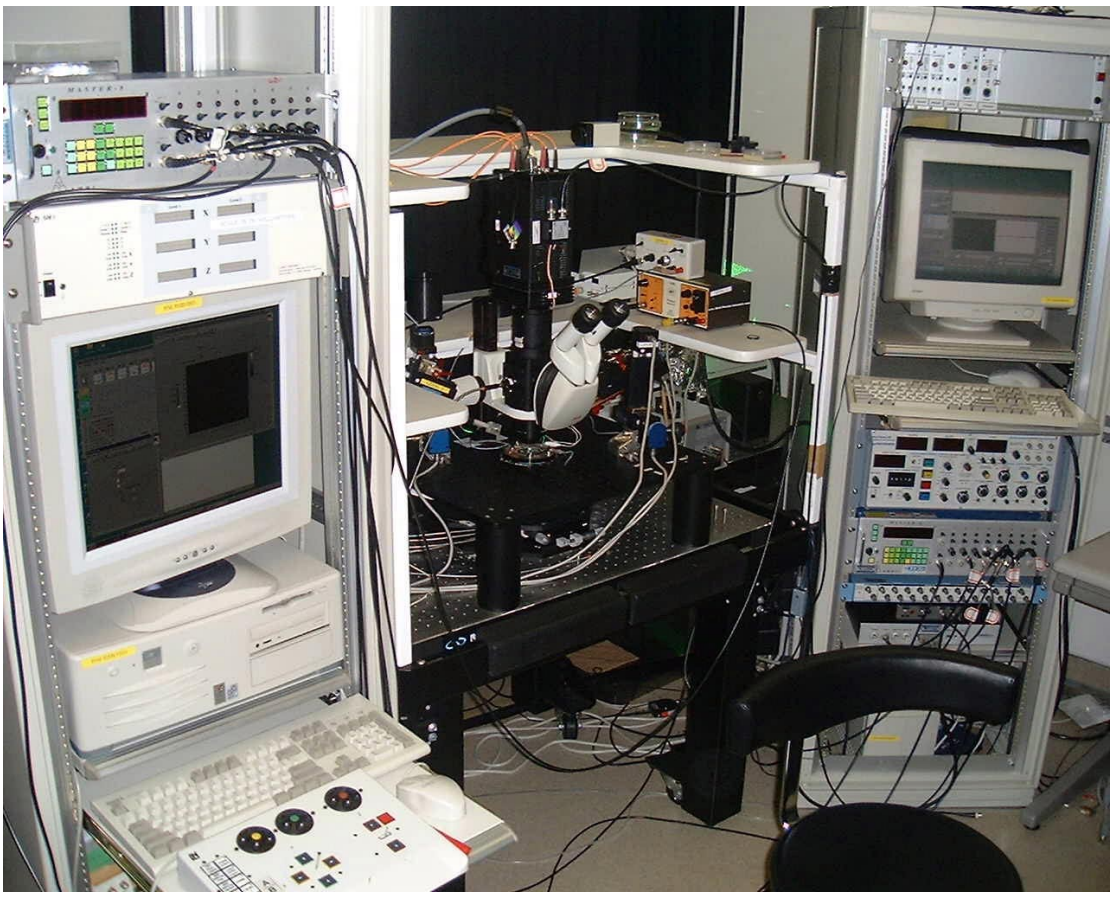

Fig. 2.4: The complete setup. The microscope and electrode manipulators sit on a vibration isolation table (center). Two cameras are controlled by two computers (MiCam, right, and PixelVision FastOne, left). A third computer (not shown) controls electrophysiology data acquisition, electrical stimulation and the timing of other components (camera, shutter, pumps, camera cooling fan) via several stimulus generators (Master 8).

is reflected by the dichroic mirror and passes through the objective onto the specimen (shown in more detail in Fig. 2.5), where it illuminates a circular area (an image of the fiber end). The diameter depends on the fiber diameter and the ratio of collimator focal length to objective focal length, usually 2mm x $f_{Objective}$ (~125 mm) / $f_{Collimator}$ (25 mm) or about 1 cm. The power incident on the specimen is in the order of a few milliwatts. Since only between one and two square millimeters of tissue are imaged by the camera and the excitation power is distributed across a 1 cm diameter disk, the necessary (utilized) excitation power is only a fraction of milliwatts.

Fluorescence generated in the specimen is collected by the objective (PLANAPO 1.6X, N.A. ~0.25, Leica), passes through the dichroic mirror, an absorption filter and a projection lens (a second inverted 1.6X objective) before hitting the CCD in the focal plane of the second objective. This results in a magnification of one. Larger and smaller magnifications (e.g. image areas) can be obtained by exchanging either the objective or the projection lens.

Two CCD cameras were used during the course of this work. The first, the BrainVision MiCAM CCD camera system uses a front-illuminated interline CCD chip (Sony ICX076AL) of 492 x 362 Pixels. Using on-chip-binning, the resolution is reduced to 90 x 60 Pixels at a maximum frame rate of 1.33 kHz. The second system, the PixelVision FastOne camera, was obtained later. It uses a back-illuminated frame-transfer CCD chip with 72 x 78 Pixels and four readout channels. The maximum frame rate is 2.7 kHz. Each pixel is 14 x 14 µm large and has a well depth of approximately 270.000 electrons, larger than

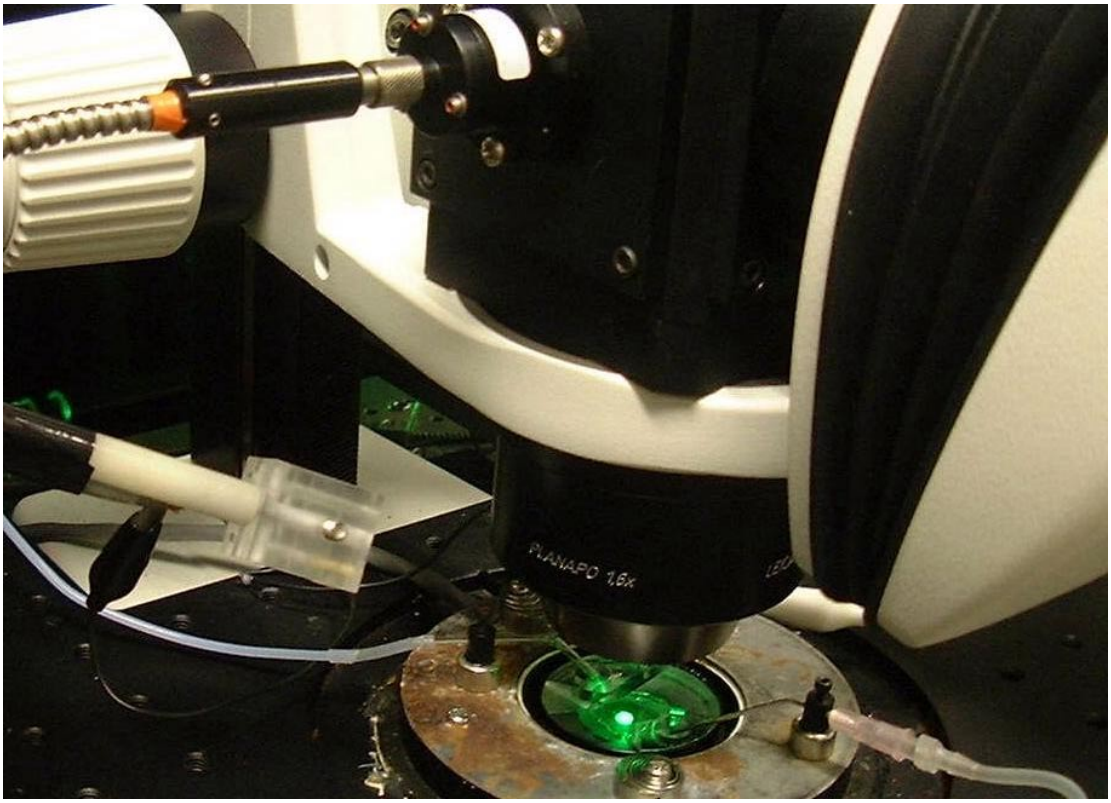

Fig. 2.5: Enlarged view of fiber collimator (upper left), objective and specimen chamber (below, empty) while the excitation light (green) is turned on.

the MiCAM system. The noise in both camera systems is dominated by photon shot noise if the CCD wells are filled to more than 50% of capacity. The PixelVision FastOne camera system has the disadvantage of using the frame-transfer method of moving the CCD image to the readout section of the CCD chip. This will result in so-called “smear” if the image is illuminated during frame transfer. This smear can be avoided by turning off the illumination while the image is transferred using the electro-optic modulator (described in Annex 1). Yet since frame transfer takes less than 10 microseconds and the current work uses changes in light intensity rather the absolute intensity as the important quantity measured, the presence of smear is unproblematic.

Due to the higher frame and the larger well depth, the PixelVision system was used preferentially. Unless noted otherwise, all optical recordings used in this work were acquired with the PixelVision system. The software designated to operate the PixelVision FastOne (designed by Red Shirt Imaging Inc.) did not allow triggering the camera with an external TTL pulse and several other software tools were developed to analyze data from the BrainVision MiCAM system. Therefore, a custom program was created under LabVIEW (version 6i, National Instruments) to permit external triggering of the PixelVision FastOne camera and save the data in the MiCAM file format for subsequent analysis. This software is described in Annex 2.

3. Functional anatomy of the cerebellum

3.1 Anatomy of the cerebellar cortex

The cerebellum is essential for all normal sensorimotor activities. It participates in all organized postural and behavioral acts. The cerebellum also plays a crucial role in the learning of simple and complex acts and skills. If the cerebellum develops abnormally, or is injured or disabled either experimentally or by disease, many striking behavioral abnormalities occur. For example, normal, everyday movements become uncoordinated and clumsy and they exhibit errors in direction, rate, amplitude, sequence and precision. In addition, fine exploratory movements and simple as well as complex coordinated act sequences are drastically impaired or lost. How the machinery of the cerebellum contributes to normal, adaptive, coordinated behavioral sequences is not well understood.

All vertebrates have a cerebellum. It lies behind the forebrain on top of the hindbrain. In birds and mammals, the surface of the cerebellum is folded into a complex arrangement of thin, elongated folia, the cerebellar cortex. Animals that have more complex behavioral repertoires are likely to have a larger and more convoluted cerebellum (Eccles et al.,1967).

The cerebellar cortex consists of a three-layered sheet of neurons containing five major types of neurons interconnected in a highly organized, specific and stereotypic way (Fig. 3.1). Two other types of neurons, Lugaro cells (Palay and Chan-Palay, 1974) and unipolar brush cells (Mugnaini and Floris, 1994) exist in smaller numbers in several folia of the cerebellum, but

are normally neglected in theories concerning the function of neuronal cell types in the cerebellum.

The Purkinje neurons have the largest cell bodies and are distributed in a single layer just beneath the outer fiber layer (molecular layer). Their axons are the only output connection of the cerebellar cortex. The thick dendrites of Purkinje cells ascend and fan out in a flattened vertical plane into the molecular layer. These flattened dendrites are arranged at right angles to the long axis of each folium and thus also to the direction of parallel fiber axons in

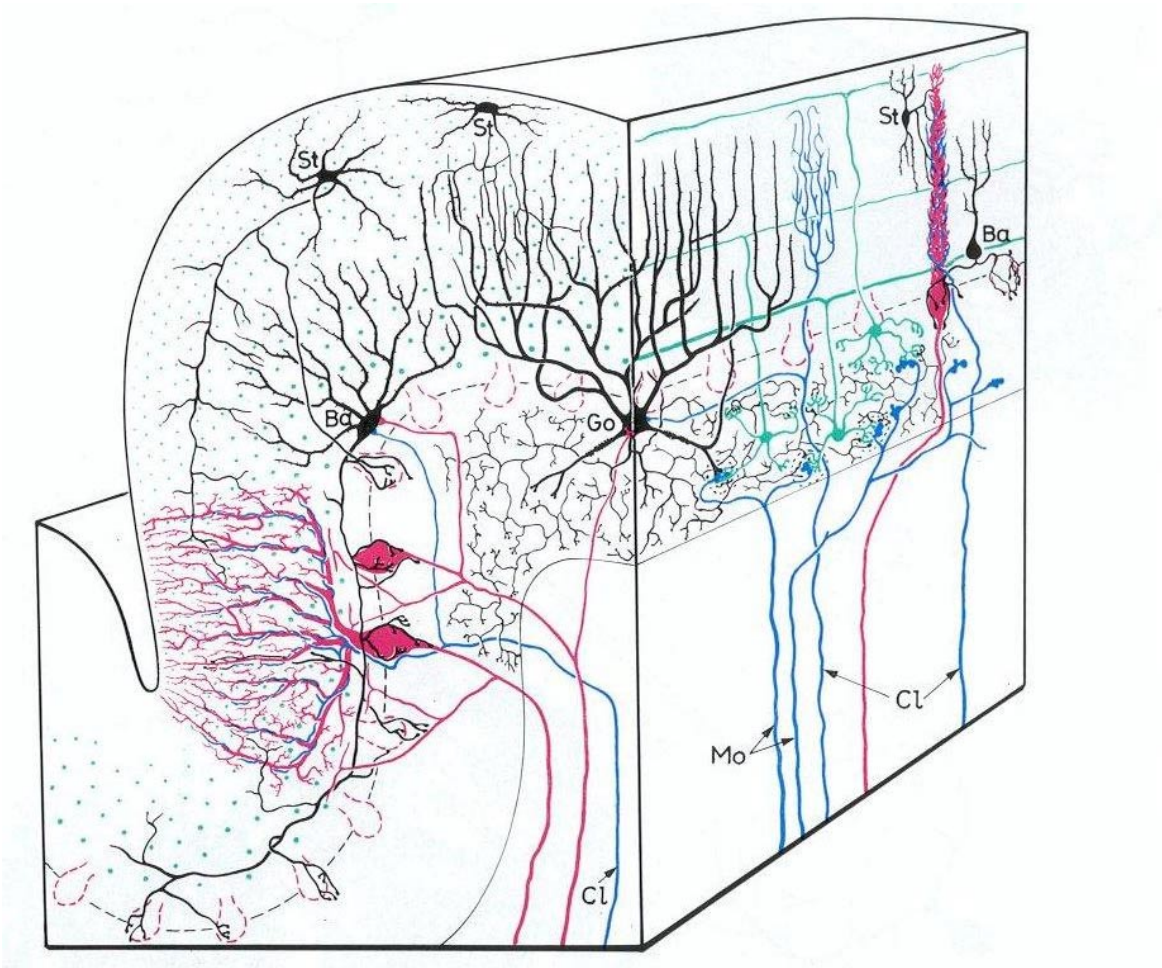

Fig 3.1: Drawing of a folium of cerebellar cortex (taken from Eccles et. al., 1967). Purkinje cells are drawn red, granule cells green, interneurons black and afferent fibers blue. See text for a detailed description.

the molecular layer. The granule cells are small, densely packed, and more numerous than all the rest of the neurons in the nervous system combined. These cells form the thick granule cell layer, and their dendrites receive most of the projections to the cerebellum from many different sources in the forebrain, midbrain, medulla and spinal cord. The axon of each granule cell ascends vertically, giving off synaptic connections to Purkinje cells. In the molecular layer, all granule cell axons bifurcate and travel horizontally within the molecular layer in both directions along the axis of the folium. These granule cell axons are called parallel fibers because they all lie in the same direction. The parallel fibers travel for variable distances and in their course they make synaptic contact with all other cell types, Purkinje cells as well as stellate cells, basket cells, and Golgi cells, all of which have their dendrites in this layer of parallel fibers. The granule cells are also the only excitatory neurons within the cerebellar cortex. The basket cells and the stellate cells are inhibitory interneurons that send their axons sideways relative to the parallel fibers. They inhibit adjacent Purkinje cells, but they do so in different spatial patterns. The Golgi cells exert feedback inhibition on localized patches of underlying granule cells.

The Purkinje cells are the sole output of the cerebellar cortex and, being inhibitory, they modulate the ongoing excitatory activity of neurons in the deep cerebellar nuclei. The excitatory activity of the deep cerebellar nuclei is projected to several thalamic and brainstem nuclear groups that are involved in sensorimotor networks. The cerebellar cortex receives input from mossy fibers and climbing fibers as well as modulatory input from monoaminergic fibers. In mammals with simple behavioral repertoires, mossy

fiber inputs to the enormous population of granule cells carry information mostly from sensory receptors on skin, muscles, tendons and other tissue throughout the body. But in behaviorally more complex mammals, the cerebral cortex contributes a greater number of cerebellar projections via the brain stem. The climbing fibers, arising from a single nucleus in the medulla called inferior olive, are a unique input in that, in the adut, they make contact only with the dendrites of Purkinje cells and each Purkinje cell is innervated by a single climbing fiber. Simultaneous activation of climbing fiber and parallel fiber input results in long-term depression (LTD) of the parallel fiber – Purkinje cell synapse, a phenomenon that is assumed to be the basis for cerebellar learning and memory (Ito, 2002).

Because the cerebellar cortex is constantly bombarded by mossy fiber input to the cortical network, complex ongoing patterns of activity are distributed throughout the cerebellar cortex in shifting spatial and temporal patterns, even during sleep (Welker, 1992). A great deal has been known about the anatomical circuitry and physiology of the cerebellar cortex for a long time. The relatively simple, almost crystalline architecture has led to great hopes of deducing how the cerebellar cortex performs its function, but so far with disappointing results (Bower, 2002). Even though lesion studies and equivalent techniques have led to a good understanding of what functions are performed by the cerebellar cortex, how the cortex and its components perform its function of timing and sequence generation is essentially unknown (Braitenberg, 2002).

3.2 The parallel fiber system

The highly regular geometrical relationship between the parallel fiber segment of the granule cell axon and the isoplanar dendrites of the overlying Purkinje cells have intrigued experimentalists and theorists for more than 100 years. The parallel fibers are probably the slowest and most numerous axons in the brain (Andersen et. al., 1992). Each parallel fiber makes a single or at most two synapses on perhaps half the Purkinje cells it encounters along its several millimeter path. The same geometry is found in all the diverse animals that have a cerebellum as well as in all the regions of the cerebellum. A parallel fiber may run for 6 mm (3 mm on each side) before coming to an end. Even though extensively folded, cerebellar cortex is a *single continuous* sheet and the only region of the nervous system to span the midline without interruption.

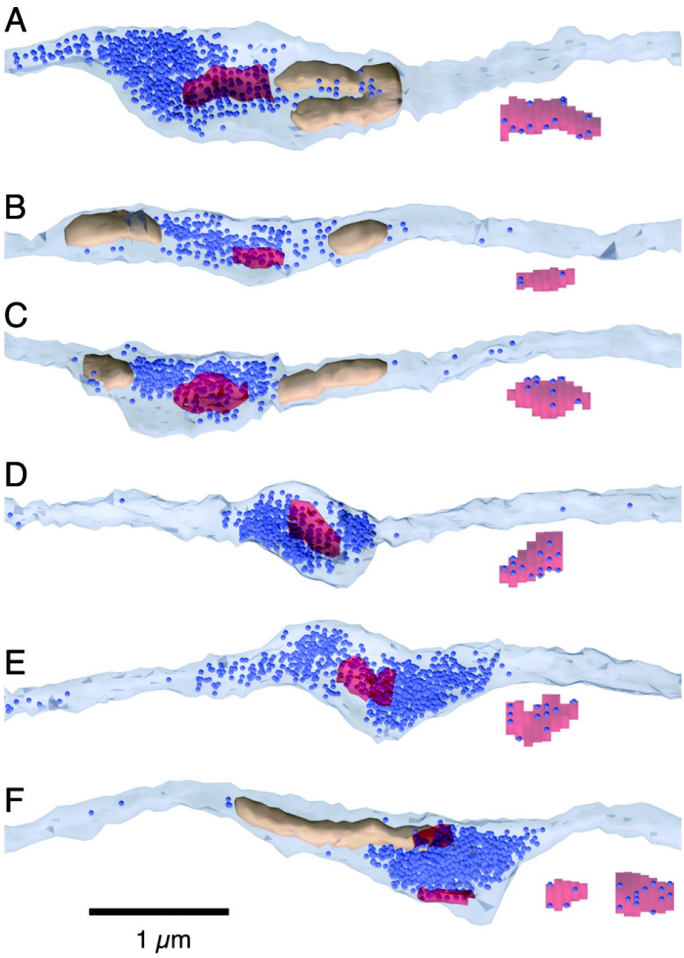

Fig. 3.2: Anatomy of six individual granule cell axons (A-F) and synaptic boutons of the rat, 3D-reconstruction from serial electron micrographs (taken from Xu-Friedmann et al.). Note the very thin axon compared to the bouton. The postsynaptic density is shown in red, mitochondria beige and vesicles in dark blue.

Each Purkinje cell is estimated to receive between 150.000 and 175.000 synapses from an approximately equal number of granule cells, the largest known synaptic convergence in the nervous system. The most prominent and now well accepted theory of cerebellar function by Marr and Albus sees this large number of synapses as the place of memory storage in the cerebellum.

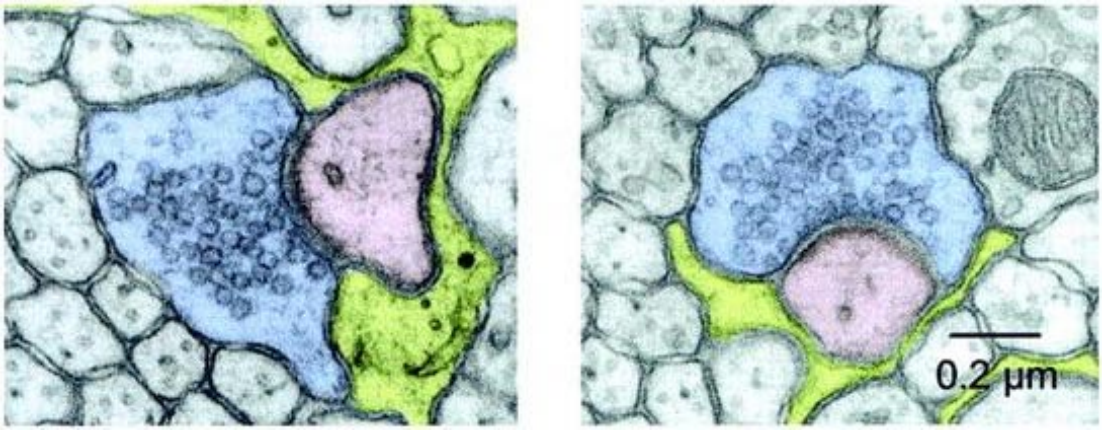

Fig. 3.3: Two parasagittal electron microscopy sections of the molecular layer containing a parallel fiber bouton (blue), the corresponding postsynaptic Purkinje cell spine (pink) and astrocyte (green) (taken from Xu-Friedmann et al.). Note the tight bundle of unmyelinated parallel fibers (axons, grey) adjacent to the bouton, their tight packaging with little extracellular space and the absence of mitochondria or vesicles.

Parallel fiber synapse strength is suppressed in response to coincident activity of the climbing fiber, which is assumed to carry an error signal. Coincident activation of climbing and parallel fibers leads to a depression in synaptic strength, while an opposite mechanism potentiates “correct” connections (Marr, 1969; Albus, 1971; for review see Ito, 2000).

The fact that a single parallel fiber sequentially contacts Purkinje cells over a distance of several millimeters also suggest that the cerebellum could

perform a timing function with the parallel fibers operating as a delay line (Braitenberg, 1987). Less obvious but equally important and crucial for such a hypothesis is the precision to which the arrangement and the conduction velocity of parallel fibers is controlled to support such a (hypothetical) function.

3.3 Description of the superficial slice preparation

Acute slices of brain tissue provide an intermediate solution between *in vivo* experiments where the brain is essentially undisturbed and *in vitro* systems such as cultures of dissociated cells. Brain slices can preserve much of the intrinsic connectivity and the tissues surrounding the cells of interest. They can be held alive for many hours *in vitro* and allow easy access with electrodes and pharmacological manipulation. In comparison to in vivo experiments, it is also much easier to record small fluorescence changes *in vitro*, due to the absence of tissue movement artifacts caused by the animals' breathing and heartbeat.

A semi-intact macro slice preparation of the mouse cerebellar cortex was prepared by dissecting the cerebellar cortex by a cut co-planar to the surface of lobules 6/7 with a maximum thickness of 400-500 micrometers. Since the cerebellar cortex is relatively thin, its internal connectivity is preserved and only long-range afferent and efferent fibers are cut.

3.4 Optical imaging of cerebellar circuit dynamics

This superficial slice preparation allowed the successful imaging and pharmacological separation of several signal components reflecting the contribution of different types of neurons in the molecular layer of the cerebellar cortex. Fig. 3.4 illustrates the two main components of the optical signal in normal artificial cerebrospinal fluid (ACSF), a large signal corresponding to activation of Purkinje cells, and a smaller signal corresponding to the compound action potential travelling along the parallel fibers. The size difference is explained by the comparatively higher membrane

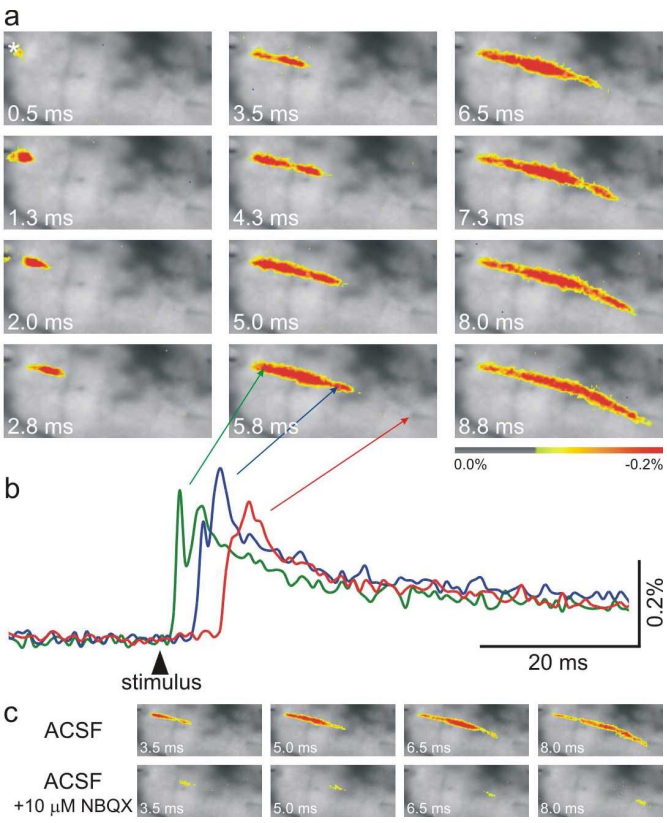

Fig. 3.4: Time series of the fluorescence images recorded after a single stimulation in the molecular layer (, 0.0 ms). Fluorescence changes above a certain threshold are color-coded and laid over the fluorescence images (image width: 2 mm). b: Fluorescence time course for three points along the activated beam, consisting of an NBQX-sensitive (postsynaptic) component (second peak) and NBQX-insensitive component (first peak, lower row in c). c: Blocking synaptic transmission with NBQX (lower panel) leaves only the presynaptic component.*

area contribution of Purkinje cells, which in this sense are the largest constituent of the molecular layer. When the surface of the cerebellum is stimulated with a train of action potentials, the signal of additional cell types

that are not activated by a single pulse can be seen. The so-called lateral inhibition (Fig. 3.5) has been observed with voltage-sensitive dyes (Cohen and Yarom, 2000) and is due to the activation of inhibitory basket and/or stellate cells, which in turn hyperpolarize Purkinje cells via GABAergic inhibitory synapses. Probably due to their small number and membrane area, activation of the inhibitory interneurons could not be detected optically. The inhibition of Purkinje cells can be separated from their direct excitation using the AMPA receptor antagonist NBQX. Fast glutamatergic transmission occurs mainly via AMPA- and NMDA-type receptors. Adult Purkinje cells express no functional NMDA receptors (Hirano and Hagiwara, 1988), while interneurons express both AMPA and NMDA receptors (Monyer et al., 1994; Carter and Regehr, 2000). Exciting the interneurons via NMDA receptors with a train of action potential while blocking Purkinje cell excitation by parallel fibers with

Fig. 3.5: Lateral inhibition and on-beam hyperpolarization. Repetitive stimulation (here 8 Pulses at 100Hz) in ACSF reveals strong excitation (yellow-red) along the beam of parallel fibers flanked by areas of hyperpolarization (blue-pink). When excitatory transmission is blocked by NBQX (middle), a strong hyperpolarization (lateral inhibition) is revealed. It is GABAergic (sensitive to picrotoxin), leaving only a weak hyperpolarization (on the beam of parallel fibers) in the presence of NBQX and picrotoxin (bottom). The image width is 2 mm.

4. Action potential generation and the role of Kv3 potassium channels

4.1 Action Potential

The Hodgkin-Huxley theory of the action potential (Hodgkin & Huxley, 1954), formulated about 50 years ago, is one of the most significant and successful models in biophysics. It was the first complete description of the excitability of a cell, constructed by empirical representation of the experimental data in a quantitative model. For the first time it linked the macroscopic level of currents

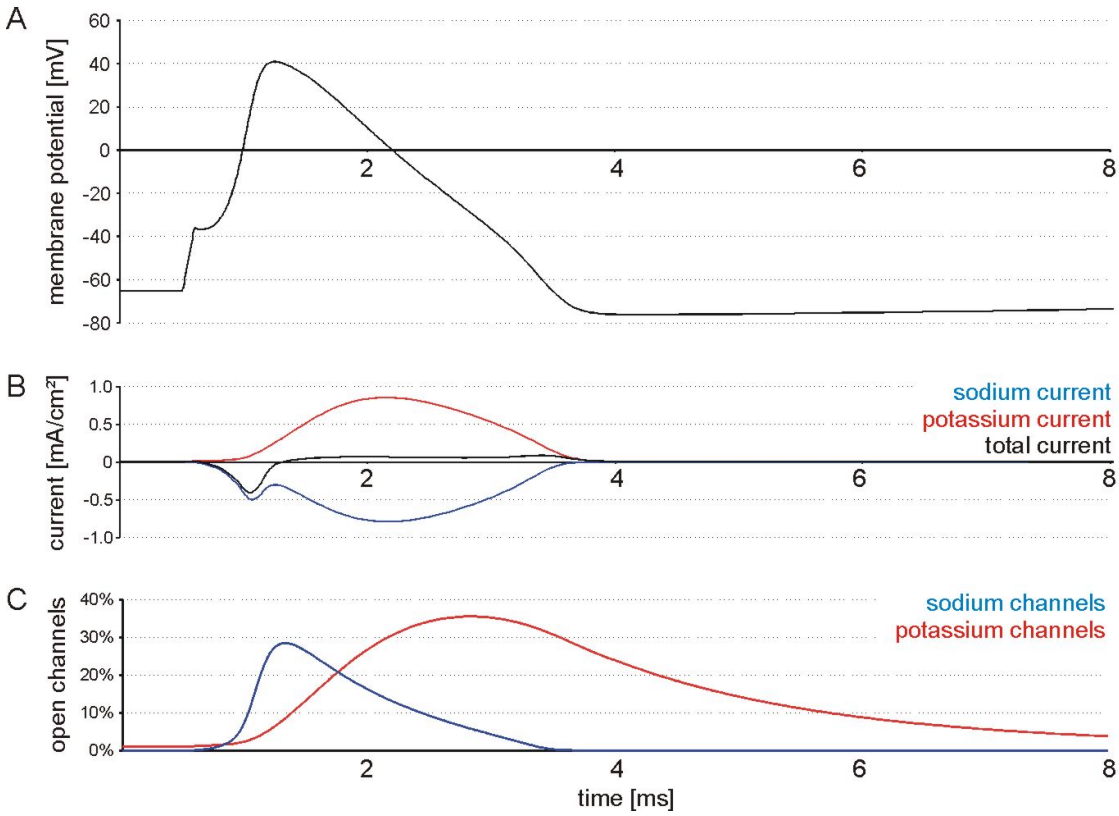

Fig. 4.1 Classic Hodgkin-Huxley squid action potential, (A) kinetics of the sodium and potassium conductances (B) and channels open probabilities (C) in sea water at 6.3°C.

and action potentials to the microscopic level of ion channels and their kinetics, which were discovered as a molecular entity only much later. A depolarizing step (done by injecting current into the axon at t=1 ms in Fig. 4.1) leads to a transient inward current followed by a sustained outward current which decays after the potential is returned to rest. By comparing traces obtained in low external sodium and traces obtained in normal sea water, Hodgkin and Huxley were able to separate total membrane current into sodium and potassium current (Fig. 4.1B). The current is related to the conductance (channel density times channel open probability) via the driving force (membrane potential minus equilibrium potential), which was modified by varying the external sodium ion concentration. The resting membrane potential is close to the potassium equilibrium potential due to higher membrane permeability for potassium. The higher permeability for potassium is due to some potassium channels open at the resting membrane potential of about -65mV (see Fig. 4.1C). The model explains a wide range of experimental phenomena, including action potential shape, propagation, spike threshold, after-hyperpolarization and the relative refractory period. Even today, almost all models of action potential generation are based on essentially the same set of equations containing channel densities, voltage-dependent gating variables and ion-dependent equilibrium potentials. This is also true for the model of granule cell axon action potential generation and propagation in chapter 6, where the factors affecting action potential amplitude, shape and conduction velocity are described in detail.

4.2 Function of Kv3 Potassium Channels

The ability to fire action potentials at high frequencies (often up to 1 kHz) or to follow high frequency inputs are important physiological functions of numerous cell types throughout the mammalian central nervous system (CNS) (Rudy and McBain, 2001). In order to fire brief action potentials in rapid succession, a cell needs action potentials that are non-decremental, of short duration, repolarize rapidly and possess brief afterhyperpolarizations. Although numerous channels types have been implicated in conferring such properties, the voltage-gated potassium channels of the Kv3 subfamily have been identified as major determinant of this 'fast spiking' phenotype (Rudy and McBain, 2001). Both rodents and humans possess four Kv3 genes: Kv3.1, Kv3.2, Kv3.3 and Kv3.4 (Rudy et. al.,1999). All four genes generate multiple protein isoforms by alternative splicing, which produces versions with different intracellular C-terminal sequences. There are now 13 different Kv3 proteins known in mammals, with 2 isoforms for Kv3.1 (Kv3.1a and Kv3.1b), and 4 isoforms for Kv3.3 (Kv3.3a-Kv3.3d). The currents expressed in heterologous expression systems by the spliced isoforms of each Kv3 gene are virtually indistinguishable (Rudy and McBain, 2001).

Cerebellar granule cells express Kv3.1,Kv3.3 and Kv3.4 mRNA (Weiser et. al., 1994; Rudy et. al.,1999). Immunohistochemical localization of Kv3.1a and Kv3.1b channel isoforms in the mouse cerebellum demonstrated strong expression of Kv3.1a and Kv3.1b protein in the granule cell axons (Sekirnjak et al., 1997;Ozaita et. al., 2002). The expression pattern of Kv3.1a

and Kv3.1b differed in the soma, but using co-immunoprecipitation assays it could be shown that most Kv3.1a protein in the cerebellum is in heteromeric complexes (channels) with Kv3.1b subunits, mostly in the granule cell axon.

All Kv3 proteins encode voltage-gated channels with a number of similar, unusual properties. Each of the four genes code for potassium channels with similar voltage dependencies (Rudy et. al.,1999). In Chinese hamster ovary cells, the currents become apparent when the membrane is depolarized to potentials more positive than approximately –20 mV, which is more depolarized than any other known mammalian voltage-gated K^+ channel by at least 10-20mV (Coetzee et. al., 1999). Another crucial property of Kv3 channels is their fast rate of deactivation upon repolarization (e. g. at –70mV Kv3.1b currents deactivate with a time constant of <1ms at room temperature), which is faster than that of any other known neuronal voltage-gated K^+ channel by about an order of magnitude (Rudy et. al., 1999, Coetzee et. al., 1999).

Kv3.1 and Kv3.2 currents are of the delayed rectifier type. Upon depolarization, currents rise relatively quickly to a maximum level that is maintained for several hundred milliseconds without inactivation. Kv3.3 and Kv3.4 currents are of the A-type, although Kv3.3 currents inactivate very slowly (inactivation time constant > 200 ms at 20 mV and 20 °C). Kv3.4 currents inactivate faster. Furthermore, inactivation of both Kv3.3 and Kv3.4 can be suppressed by phosphorylation of the inactivation gate by protein kinase C (Covarrubias et. al., 1994).

4.3 Kv3.1/Kv3.3 double knockout mice

Mice in which the genes encoding Kv3.1 and Kv3.3 are individually inactivated have been generated first (Chan, 1997; Ho et. al., 1997). The Kv3.1 single mutant showed increased γ- and decreased δ-oscillations and a motor-skill deficit caused by altered muscle contractility and force generation (Ho et. al.,1997; Joho et. al., 1997, 1999). The motor-skill deficit is, however, only present in 129/Sv and not in 129/Sv x C57BL/6 F1 mice; i.e. the penetrance of the Kv3.1-null mutation depends strongly on the genetic background (Sanchez et. al., 2000). The Kv3.3 single mutant displays no overt phenotype (Chan, 1997). The relatively weak phenotype obtained in Kv3.1 or Kv3.3 knockout (KO) mice and resilient fast spiking in GABAergic interneurons of Kv3.1 knockout mice suggested redundancy in the action potential repolarization mechanism of these neurons (Porcello et. al., 2002). The wide coexpression of Kv3.1 and Kv3.3 was assumed to be the cause for this, as Kv3.3 could be capable of assuming some of the functions of Kv3.1 in Kv3.1 KO mice and vice versa.

Kv3.1 and Kv3.3 double knockout (DKO) mice could be obtained by crossing double-heterozygous (Kv3.1$^{+/-}$ Kv3.3$^{-/+}$) with Kv3.3 KO mice. The loci Kcnc1 and Kcnc3 encoding Kv3.1 and Kv3.3 K^+ channel subunit are located close to each other on chromosome 7 in the mouse. A spontaneous recombination event on chromosome 7 was detected after about 100 offspring. The resulting chromosome lacking both Kv3.1 and Kv3.3 could then be used to obtain (25%) double knockout (Kv3.1$^{-/-}$ Kv3.3$^{-/-}$) mice from crossing double-heterozygous (Kv3.1$^{+/-}$ Kv3.3$^{+/-}$) (DHET) mice.

Mice lacking both the Kv3.1 and Kv3.3 potassium channels display several immediately recognizable phenotypes such as tremors, severe ataxia and spontaneous myoclonus (brief, involuntary muscle contractions, whole-body jerks) every few seconds when at rest. Furthermore, they are hyperactive, hypersensitive to alcohol and show increased exploratory activity. That Kv3.1/3.3 DKO mice were born at the expected Mendelian frequency (25%) showed that neither Kv3.1 nor Kv3.3 are essential for embryonic development. The DKO phenotype becomes apparent at postnatal day 7, with DKO mice being clearly smaller than double-heterozygeous (DHET) and wild-type (WT) littermates. When the competing DHET and WT littermates were removed and DKO mice were provided with soft food, ~80-90% survive to adulthood, albeit reaching only ~50-60% of the body weight of WT or DHET mice. DKO gross brain anatomy is normal. The mutant cerebellum shows an unchanged appearance of the molecular, Purkinje cell, and granule cell layers, including normal foliation and cytoarchitecture (Espinoza et. al.,2001). DKO mice also show normal learning and memory in an active avoidance task.

Several of the observed phenotypes that are normally associated with deficits or abnormalities of the cerebellum such as ataxia, tremor, myoclonus and ethanol sensitivity show penetrance only in the Kv3.1/3.3 -/-,-/- (double knockout, DKO) mice, whereas others such as spontaneous locomotion and center-field occupancy show penetrance already in DHET animals (Espinoza et al., 2001). This, together with the absence of a cerebellar phenotype in single mutants, led to the hypothesis that a cell type co-expressing Kv3.1 and Kv3.3 should be the deciding factor causing the double knockout phenotype.

5. Experimental Results

5.1 Optical recording analysis methods

Optical recordings of the propagating action potential were obtained from three different mouse genotypes: 1. wild type (Kv3.1 +/+ Kv3.1 +/+) mice, 2. Kv3.1 -/- (KO) Kv3.3 +/- (heterozygous, HET) mice and 3. Kv3.1 -/- Kv3.3 -/- (double knockout, DKO) mice. Optical recordings were obtained as described in Chapter 2, i.e. from slices of the surface of the cerebellar vermis of lobule

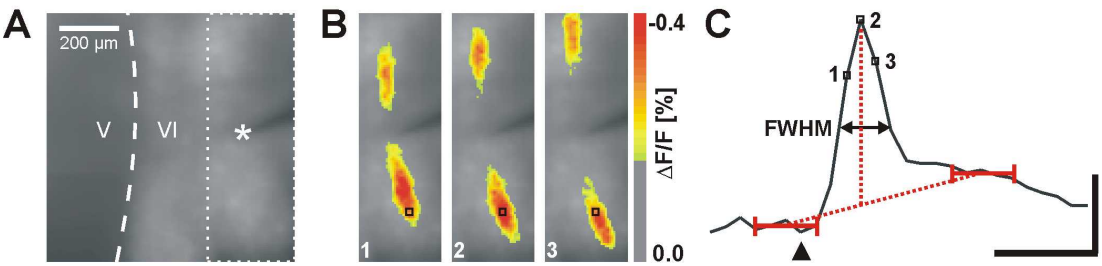

Fig. 5.1: Principle of optical recording data analysis (A) Fluorescence image of the lobule V & VI cerebellar surface stained with the voltage-sensitive dye. The stimulation electrode (*) was placed in the molecular layer of lobule VI. (B) Color-coded fluorescence change 1.11ms (1) , 1.48ms (2) and 1.85ms (3) after stimulation. Membrane depolarization is recorded as a fluorescence decrease (yellow-red). Two action potential volleys can be seen propagating in tranversal direction (along the parallel fibers) from the point of stimulation. (C) Inverted Fluorescence time course at the point marked by a black square in (B). Numbers 1-3 correspond to the fluorescence 1.11ms (1) , 1.48ms (2) and 1.85ms (3) after stimulation (frames shown in (B)). Action potential width is measured at half maximum fluorescence change (full width at half maximum, FWHM) relative to a baseline (red, dotted), which is the mean of 10 pixel values recorded 3-7 frames before and 6-10 frames after peak fluorescence. The stimulation time point is marked by a black triangle. Calibration bars are 2 ms and 0.2%, respectively.

6/7 stained with di-4-ANEPPS and recorded using the PixelVision FastOne camera. Synaptic transmission was blocked by adding NBQX (10μM) and bicuculline (20μM) to the bath solution. A principal overview of how optical recording data was analyzed is shown in Fig. 5.1.

Due to the huge number of data points available, automatic data analysis was implemented in Interactive Data Language (IDL 5.4, Research Systems). Fluorescence images were filtered with a 3 x 3 (42 μm x 42 μm) box filter. The procedure was repeated for each pixel independently. The amount of noise present in each location in the image area was quantified by calculating the standard deviation of 15 fluorescence values preceding the first stimulation by 3-17 frames (1.11-6.29ms). To determine whether a certain location contains data (contains an action potential propagating through this location), a peak fluorescence amplitude of more than 12 standard deviations was chosen as the criteria to determine if an action potential propagated through the location corresponding to the pixel analyzed). The peak fluorescence decrease during the time an action potential could have propagated through in the image (from stimulation to a few milliseconds after stimulation) was measured. The fluorescence baseline for each peak (in a series of stimulations) was obtained as the average of 10 fluorescence values, 5 preceding the action potential peak by 3-7 frames (1.11-2.59ms) and 5 values 6-10 frames (2.22-3.7 ms) after stimulation. If peak fluorescence minus the fluorescence baseline was greater than 12 standard deviations (i.e. the signal-to-noise ratio was greater than 12), the pixel was scored as a valid data point for further analysis. Figure 5.2 shows an example of the peak frame number and the local signal-to-noise ratio.

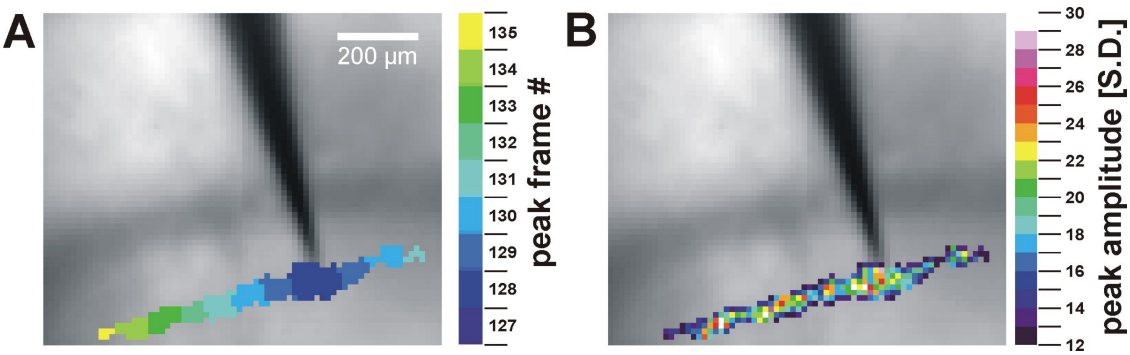

Fig. 5.2: Determination of valid data points. (A) Frame number of peak fluorescence change. (B) Peak amplitude in standard deviations. Only valid data points (pixels) with a peak amplitude of more than 12 standard deviations are color-coded. The gray background image is the raw fluorescence intensity

The calculation of the fluorescence baseline was sometimes necessary to correct for slow changes in fluorescence not due the action potential, mostly on-beam hyperpolarization (described in chapter 4). Fluorescence bleaching would also be corrected for in this way, but was always negligible.

5.2 Action potential width

The time points of action potential rise and fall above and below half maximum were calculated using linear interpolation between the fluorescence values for each frame. The difference between rise time point and fall time point was taken as the action potential width (full width at half maximum, FWHM). Only data points with unequivocal rise and fall time points were included in the analysis. Figure 5.3 shows 3 examples (one genotype each), “maps“ of the action potential width obtained in this way.

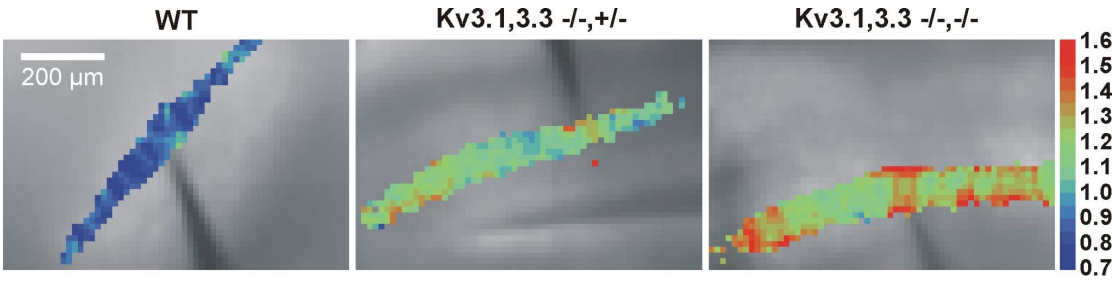

Fig. 5.3: Color-coded maps of the action potential width. The color scale (right) shows the corresponding action potential width in milliseconds.

As can be seen in Figure 5.3, the action potential becomes gradually broader as the number of alleles encoding Kv3 channels is reduced. To compare the distribution of action potential width for each genotype, all valid data points from different experiments/animals were pooled into three groups for WT (n=7 animals), Kv3.1 -/- Kv3.3 +/- (n=6 animals) and DKO (n=7 animals). Fig. 5.4 (A) shows the result in a histogram. To test for the statistical significance of the difference between genotypes, the mean action potential width was calculated for each animal. Figure 5.4 (B) shows the average action potential

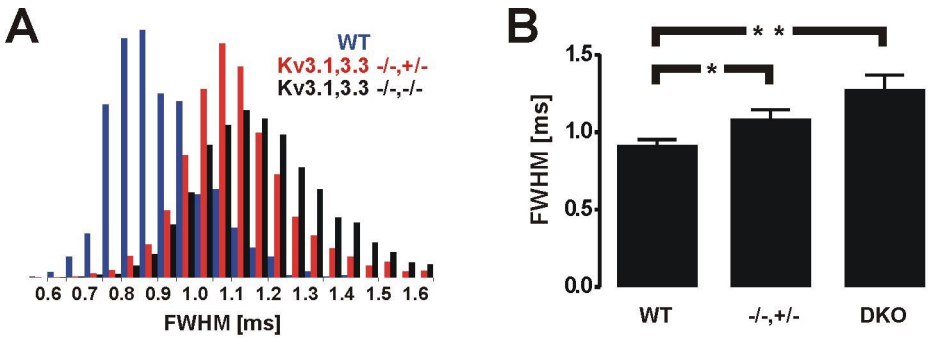

*Fig. 5.4: Histogram of action potential widths (A) and mean action potential width (B) (mean ± s.e.m.) for WT (917±36 µs, n=7), Kv3.1/3.3 -/-,+/- (1088±56 µs, n=6) and Kv3.1/3.3 -/-,-/- (1280±89 µs, n=7). Brackets indicate significant differences (*: p<0.05; **: p<0.01).*

width for each genotype. The p-values for statistical significance between the groups of genotypes were calculated using students t-test.

5.3 Conduction velocity

Looking at the color-coded frame number of peak fluorescence change (example in Fig. 5.2 A), it seemed that the band of color were wider in DKO mice than in WT mice. This suggested that the conduction velocity was higher in DKO mice. Conduction velocity can be quantified using the spatio-temporal information provided by the imaging data, measured by plotting the distance an action potential traveled against time. Time was defined as the time interval between stimulation and rise time point of the action potential and distance as the distance of the data point from the point of stimulation (Fig. 5.5). The point of stimulation was defined as the center of gravity of the group

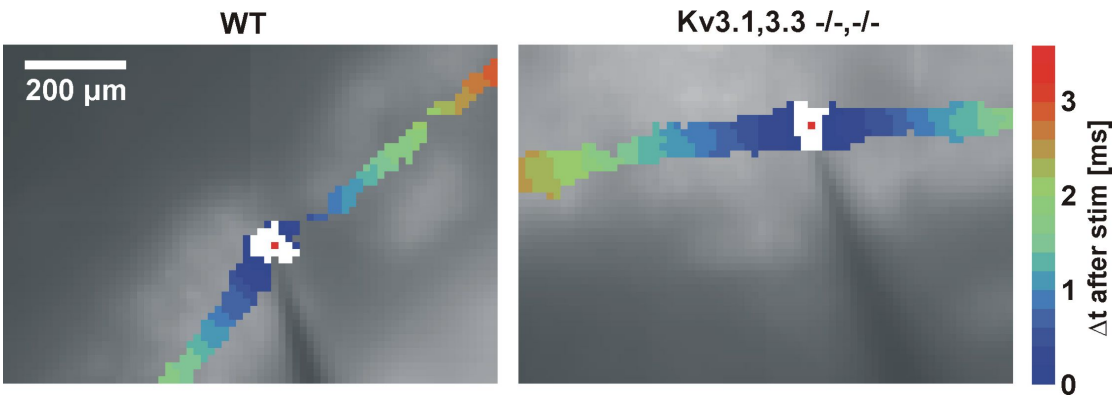

Fig. 5.5: Maps of the delay between stimulus and action potential rise above half maximum in a WT and a Kv3.1/3.3 -/-,-/- mouse. The action potential propagates from the stimulation area (white, with center marked red) at approximately constant speed.

of 25 data points that had the earliest rise time point. These 25 data points closest to the stimulation point were not included when determining conduction velocity. Conduction velocity was defined as the slope of the first-order linear regression line. Only animals where the time range of valid data points spanned more than 1 ms were accepted for statistical analysis. For statistical significance, conduction velocities between groups of animals of the respective genotypes were compared using Students t-test. Fig. 5.6 shows a plot of time against distance traveled (Fig. 5.6.A) and a bar graph showing the increased conduction velocity in mice lacking Kv3 alleles.

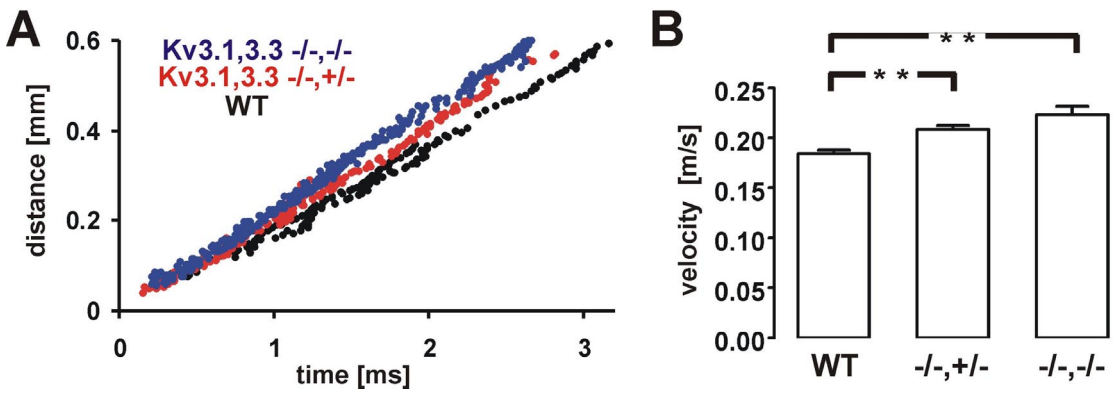

Fig. 5.6.: (A) Rise time points of individual AP data points plotted against the distance from the origin of stimulation for a WT, Kv3.1/3.3 -/-,+/- and Kv3.1/3.3 -/-,-/- mouse. (B) Parallel fiber conduction velocity is significantly increased from 184 ±3 mm/s (mean ± s.e.m., n=5) in WT to 208 ±4 mm/s in Kv3.1/Kv3.3 -/-,+/- (n=4, p<0.01) and 223±8 mm/s (n=4, p<0.01) in Kv3.1/Kv3.3 -/-,-/- mice.

5.4 Effects of Kv3 antagonists on action potential shape

Tetraethyl-ammonium (TEA) is a potent antagonist to a variety of potassium channels. All Kv3 channels are very sensitive to TEA, and Kv3 currents are blocked > 80 % by 1mM TEA (Vega-Saenz de Miera et. al., 1994;Rudy et. al.,

1999). This sensitivity makes TEA the antagonist of choice for Kv3 channels , as this concentration produces significant inhibition of only a few other known potassium channels, among them Kv1.1 (Coetzee et. al.,1999), which might be present in parallel fibers (Wang et. al.,1994;Veh et. al.,1995).

Acute application of TEA can be used to discriminate whether the observed difference in the action potential width was the direct consequence of the absence of Kv3.1 and Kv3.3 potassium channels and not due to possible secondary changes caused by their absence. The effect of TEA should be negligible (or very small) in KV3.1/Kv3.3 DKO mice, and increase as the expression of Kv3 currents increases.

After recording the action potential shape in normal recording solution (ACSF + 20 µM NBQX + 20 µM bicuculline) at different stimulation rates, the measurements were repeated in the presence of 1 mM TEA in the external solution. Fig. 5.7 shows the effect of TEA on action potential shape in

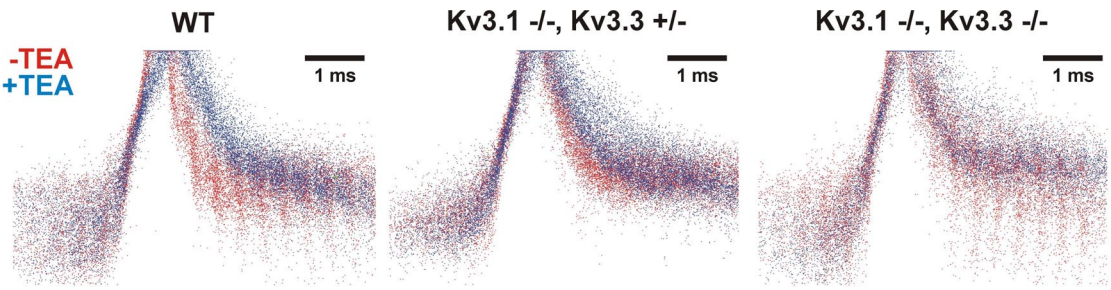

Fig. 5.7: Effect of TEA on individual action potential shape. TEA causes a large broadening of action potential shapes in WT, whereas in the DKO, no apparent difference between AP shapes in the presence (blue) or absence (red) of TEA can be seen. Broadening induced by TEA is significant ($p<0.01$) in the WT(n=6 animals) and in Kv3.1 -/-, Kv3.3 +/- animals (n=6), whereas changes in the DKO (n=4) are not significant.

the different genotypes. TEA has a large effect on action potential shape in WT, whereas in Kv3.1 -/-, Kv3.3 +/- and in DKO mice, the effect is smaller. This replicates previous results that TEA has a strong effect on action potential shape (in WT), and (indirectly) confirms the expectation that TEA-sensitive potassium channels are largely absent in DKO mice

5.5 Impaired high frequency firing in Kv3 knockout mice

Previous research has shown that the presence of Kv3 potassium channels is very important for the ability to fire action potentials at high frequency in several types of cells. In auditory neurons, modulation of Kv3 function by the antagonist TEA (Wang et. al.,1998), genetic knockout of Kv3.1 (Macica et. al., 2003) or by preventing phosphorylation with inhibitors of the phosphorylating protein kinase CK2 (Macica et. al., 2003) impaired high frequency firing. Similarly, application of TEA affected high frequency firing in cortical interneurons (Erisir et. al.,1999; Rudy et. al.,1999). The function of the Kv3 channel is to rapidly repolarize the soma (or axon) , so that sodium channels can recover from inactivation fast. Furthermore it is important that the potassium channel deactivates rapidly so that small depolarizing currents can increase the membrane potential to threshold. Open potassium channels would efficiently shunt a structure, preventing a large enough depolarization of the membrane.

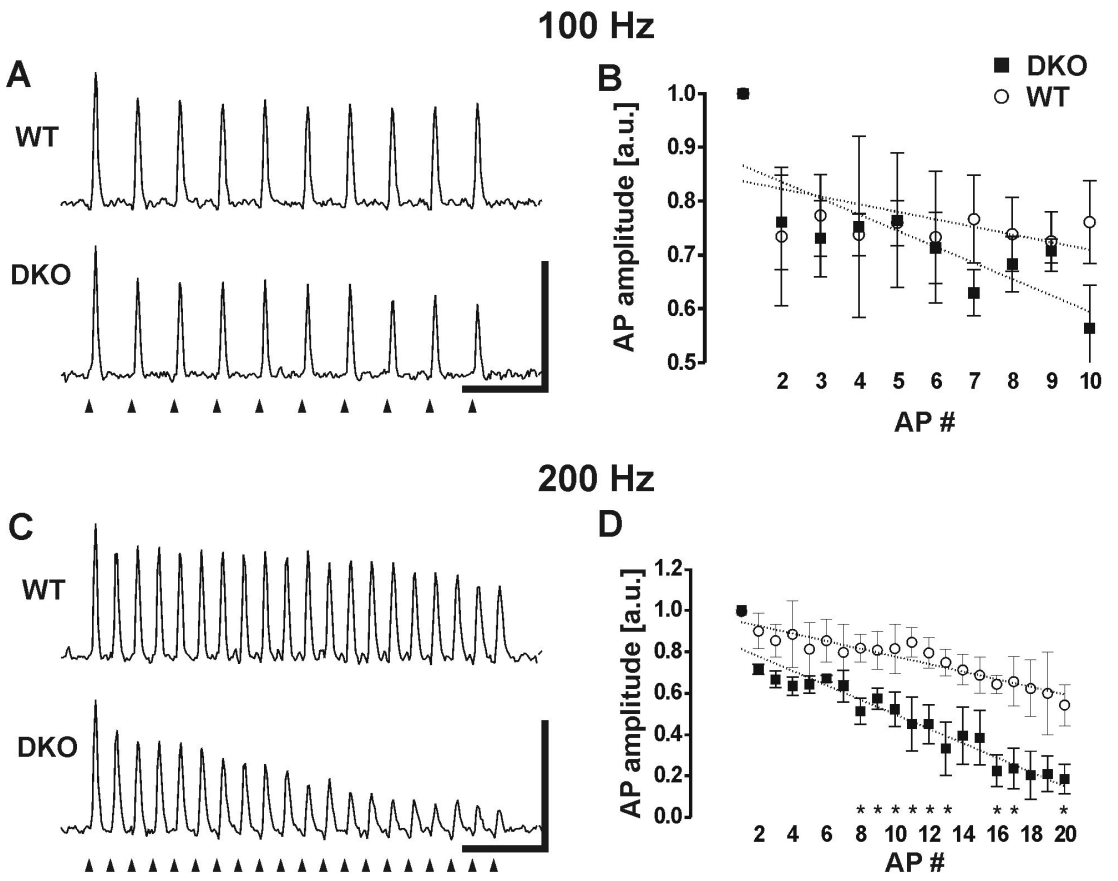

Fig. 5.9: High-frequency firing: Fluorescence timecourses (A&C) were obtained by subtracting a baseline (4.44 ms moving lower quartile) from the raw fluorescence measurements, removing slow components such as on-beam hyperpolarization. Calibration bars: 20 ms, 0.2%. To compare the AP signal size (B&D), peak heights were normalized relative to the maximum peak height. (usually the first pulse). Students t-test was used to test statistical significance. Asterisks mark significant differences ($p < 0.01$).

Figure 5.9 shows that both Kv3.1/3.3 double knockout and WT mouse parallel fibers could conduct action potentials at 100Hz faithfully, with only a small amplitude reduction in DKO relative to WT at the end of the train of 10 pulses. Since conduction of an action potential is an all-or-nothing event, a reduction in optical signal size mainly reflects a decrease in the number of fibers conducting an action potential (the signal is the sum of the signal from many

fibers) and not a decrease in action potential (membrane potential) amplitude, which remains almost constant during high frequency firing (see also chapter 6). When stimulated at 200Hz however (Fig. 5.9C), it is apparent that the DKO axons cannot sustain firing at 200Hz nearly as faithful as the WT. WT axons reliably conduct APs even at 200Hz with relatively little reduction in amplitude (Fig. 5.9D), whereas in the DKO, conduction failures are close to 80% for the last of 20 pulses at 200Hz.

Cerebellar granule cells receive high frequency input from mossy fibers (Kase et al.,1980). They are regularly firing neurons which do not show adaptation (D'Angelo et al., 1995, Brickley et al. 1996) and can fire at frequencies above 100 Hz *in vitro* (Gabbiani et al., 1994). They are assumed to be sparsely coding, i. e. to have a low average firing rate, but to fire vigorously upon coincident activation of afferent mossy fibers. Recordings from granule cells *in vivo* are rare due to their small size, but recently such recordings have been obtained using whole cell patch clamp recording of granule cells in unanaesthetized, decerebrated cats (Jorntell and Ekerot, 2003). Intense bursts of spikes (up to 1000 Hz) have been observed *in vivo*, while the other assumptions about granule cell function have been largely confirmed. The observed impairment in the transmission of high frequency firing should therefore disturb granule cell function considerably by decreasing the range of the linear input (inward current) – output (firing rate) relationship (D'Angelo et al., 1995).

5.6 Electrophysiological results

Electrophysiological recordings from cerebellar Purkinje cells were obtained using standard patch-clamp recording methods described in detail elsewhere (Hamill et. al., 1981; Edwards et. al., 1989). Parasagittal cerebellar slices (200µm) were prepared from 20-22 day old mice following previously established techniques (Tempia et. al.,1998). Whole-cell recordings were obtained from Purkinje cells visualized using a 40X water-immersion objective in an upright microscope (Zeiss). Pipettes were pulled from borosilicate glass and had a resistance of 2-4 MΩ when filled with internal solution. The internal solution contained either (in mM) 140 KGluconate, 10 HEPES, 4 $MgCl_2$, 0.5 EGTA, 4 Na-ATP, 0.5 Na-GTP adjusted to pH 7.3 using KOH or 130 CsCl, 10 TEA, 10 HEPES, 4 $MgCl_2$, 1 EGTA, 4 Na-ATP, 0.5 Na-GTP adjusted to pH 7.3 using CsOH. The cells were recorded with an Axopatch amplifier (Axon Instruments, Foster City, CA). A glass pipette pulled from sodalime glass (tip diameter 3-10 µm) was filled with ACSF and positioned in the molecular layer. Current pulses (200µs, 2-30µA) were used to stimulate the parallel fibers.

5.6.1 Paired-pulse facilitation

The shape of the presynaptic action potential is of fundamental importance in determining the strength and reliability of synaptic transmission, and altering the presynaptic waveform has been shown to affect neurotransmitter release in many systems (Augustine, 1990; Sabatini & Regehr 1999). Lack of Kv3.1

and Kv3.3 channels broadens the action potential through slower AP repolarization (Fig. 5.3 & 5.7). At the synapse between granule cells and Purkinje cells, a slight broadening of the presynaptic AP modestly increases presynaptic calcium influx by increasing the average open time of calcium channels (Sabatini et al., 1997). The relationship between AP width and calcium influx is approximately linear (Sabatini et al., 1997; Geiger & Jonas, 2000), but subsequent neurotransmitter release and EPSCs show a supralinear (Hill coefficient >2) relation to calcium influx.

At many synapses, when two action potentials depolarize a presynaptic bouton in rapid succession, the second action potential induces a larger release of neurotransmitter than the first (Magleby, 1987; Zucker, 1989). This short-term enhancement of release that persists for tens to hundreds of milliseconds after a conditioning pulse is known as facilitation. Facilitation (the increase in transmitter release/EPSC amplitude) is caused by increased release probability (Katz and Miledi, 1968, Atluri and Regehr, 1996) and changes in paired-pulse facilitation are usually considered as an indicator of alterations in presynaptic transmitter release (Manabe et al., 1993). Facilitation is crucially dependent on presynaptic residual calcium (Ca_{res}) (Zucker, 1999, Zucker and Regehr, 2002). In contrast to the high calcium levels that trigger transmitter release after a presynaptic action potential (>10 µM for ~1 ms), Ca_{res} is the modest elevation in calcium levels (hundreds of nanomolar) lasting hundreds of milliseconds. During high frequency presynaptic activity, residual calcium accumulates in the axon, causing increased release probability during subsequent APs (Dittman et al. 2000). Parallel fiber-Purkinje cell synapses are assumed to have a low initial

probability of transmitter release. Paired-pulse facilitation is reduced at this synapse by increasing calcium influx during an AP, which can simply be achieved with an increased extracellular calcium concentration (Kreitzer and

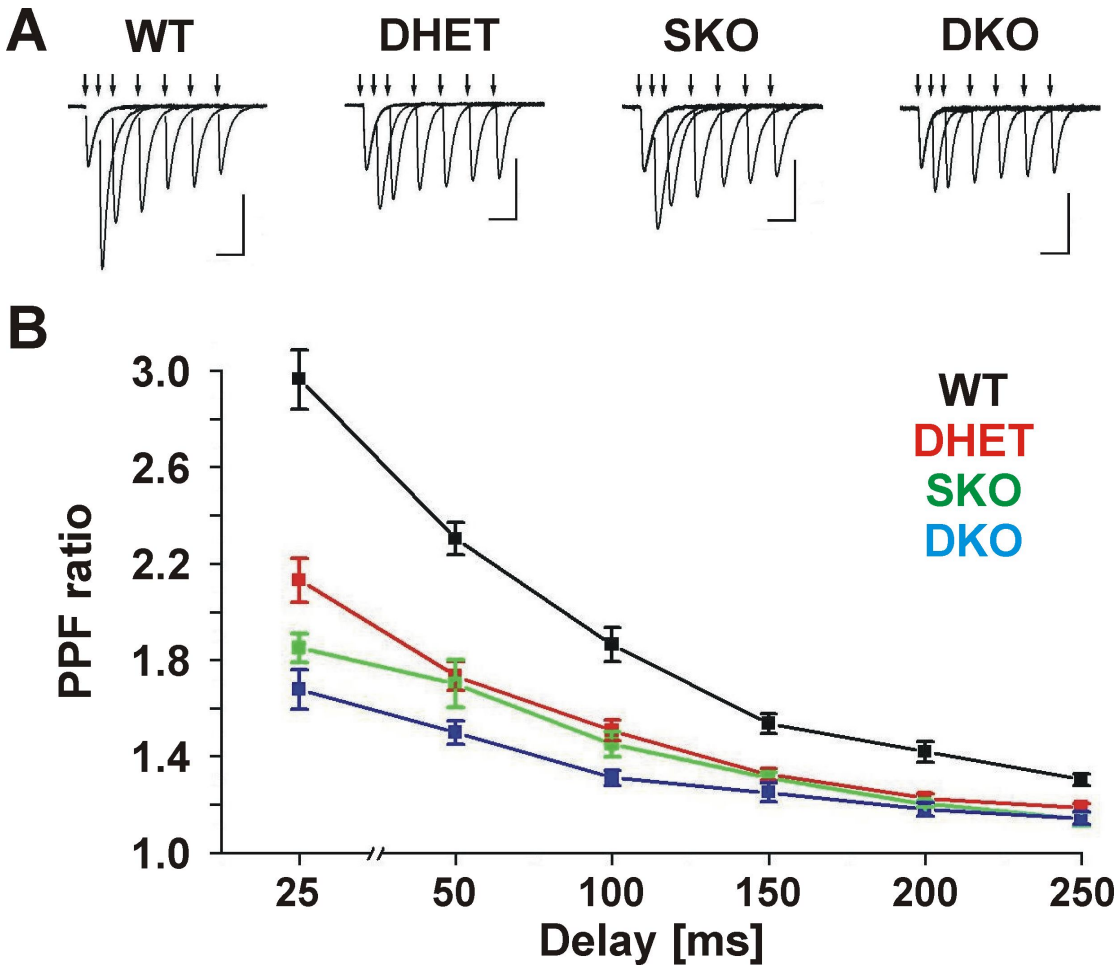

Fig. 5.10: Short-term plasticity is altered in mice lacking Kv3.1/3.3 alleles. (A) Example traces showing Purkinje cell EPSC paired pulse facilitation at intervals of 25, 50, 100, 150, 200 and 250ms in wild type, Kv3.1/3.3 -/-,+/+ (SKO), Kv3.1/3.3 +/-,+/- (DHET) and Kv3.1/Kv3.3 double knockout (DKO) mice. Vertical arrows mark electrical stimulation, stimulation artifacts have been suppressed. Calibration bars: 100 ms, 200 pA. (B) EPSC paired pulse facilitation is reduced gradually by lack of Kv3.1 or Kv3.3 alleles. Kv3.1 KO and Kv3.1/3.3 DHET is indistinguishable for all paired pulse delays investigated (wild type N=8 animals, n=26 cells; Kv3.1/3.3 DKO N=8,n=33; Kv3.1 KO N=3,n=22; Kv3.1/3.3 DHET N=4,n=23).

Regehr, 2000). The prolonged action potential should therefore reduce facilitation because a prolonged action potential will increase calcium influx. Measurement of paired-pulse facilitation by recording AMPA receptor mediated excitatory postsynaptic currents (EPSCs) from Purkinje cells in whole cell configuration (Fig. 4A-D) therefore provided an easy test to confirm the effect of increased action potential duration. Paired pulse facilitation is quantified as the ratio of the delayed (second) peak excitatory postsynaptic current (EPSC) to the undelayed (first) EPSC. At a paired-pulse interval of 50ms, mice lacking Kv3.1 or Kv3.3 alleles exhibited a significant reduction in paired-pulse facilitation of parallel-fiber mediated EPSCs from 230% in WT to 173% in Kv3.1/3.3 +/-,+/-, 170% in Kv3.1/3.3 -/-,+/+ and 150% in Kv3.1/Kv3.3 double knockout. Similar reductions were observed at intervals of 25ms, 100ms, 150ms, 200ms and 250ms (Fig. 5.10B). Statistical differences between the paired pulse facilitation of the different genotypes at a delay of 100 ms are shown in a bar chart (Fig. 5.11). WT and DKO are significantly different from all other genotypes, while DHET and SKO are statistically indistinguishable.

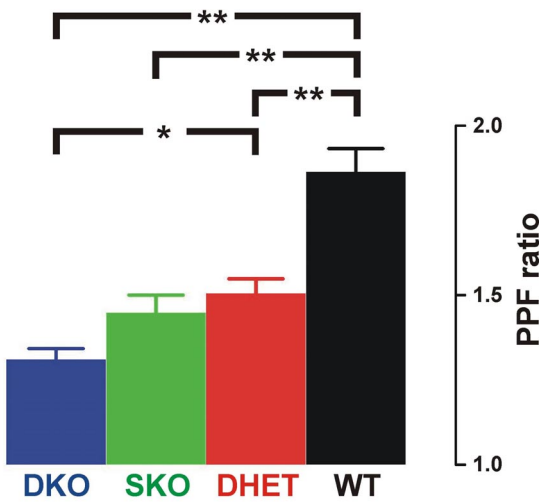

*Fig. 5.11: Bar chart of paired pulse facilitation (second EPSC delay: 100 ms) and statistical significance of differences (**:P < 0.01; *:P < 0.05).*

Based on the FD model for facilitation and depression (Dittman et al. 2000) at this synapse, the reduction in facilitation is explained by the increase in initial release probability. The increase in release probability for the second action potential caused by residual calcium is relatively reduced.

5.6.2 Induction of mGluR-mediated potentials

Synaptic signaling at the parallel fiber – Purkinje cell synapse involves two types of receptors: AMPA receptors for fast synaptic transmission and a metabotropic glutamate receptor, mGluR1, which mediates a slower phase of excitation (Batchelor et al.,1994; Batchelor and Garthwaite, 1997; Tempia et al.,1998). Unlike AMPA receptors, which sit on the postsynaptic density opposite the parallel fiber release sites, the highest density of mGluR1 is located perisynaptically (Baude et al., 1994; Petralia et al., 1997;Mateos et al.,2000). High frequency stimuli are necessary to activate mGluRs at parallel fiber synapses (Batchelor et al.,1997; Finch and Augustine, 1998; Tempia et al., 1998). This led to the assumption that glutamate spillover into the perisynaptic region is required for the induction of mGluR1-mediated currents, and indeed glutamate uptake by glutamate transporters located close to the mGlurRs controls the expression of mGluR-mediated currents in cerebellar Purkinje cells (Reichelt and Knöpfel, 2002; Brasnjo and Otis, 2001). Activation of mGluRs is also necessary for the induction of LTD (Linden et al., 1991; Aiba et al., 1994; Conquet et al., 1994; Ichise et al.,2000), which is also affected by changes in glutamate uptake (Brasnjo and Otis, 2001).

An increased release probability in mice lacking Kv3 alleles could affect the induction of mGluR1-mediated currents by increasing spillover into the perisynaptic region at an equal number of stimuli and as a consequence alter the induction of synaptic plasticity in these mice. To test whether the induction

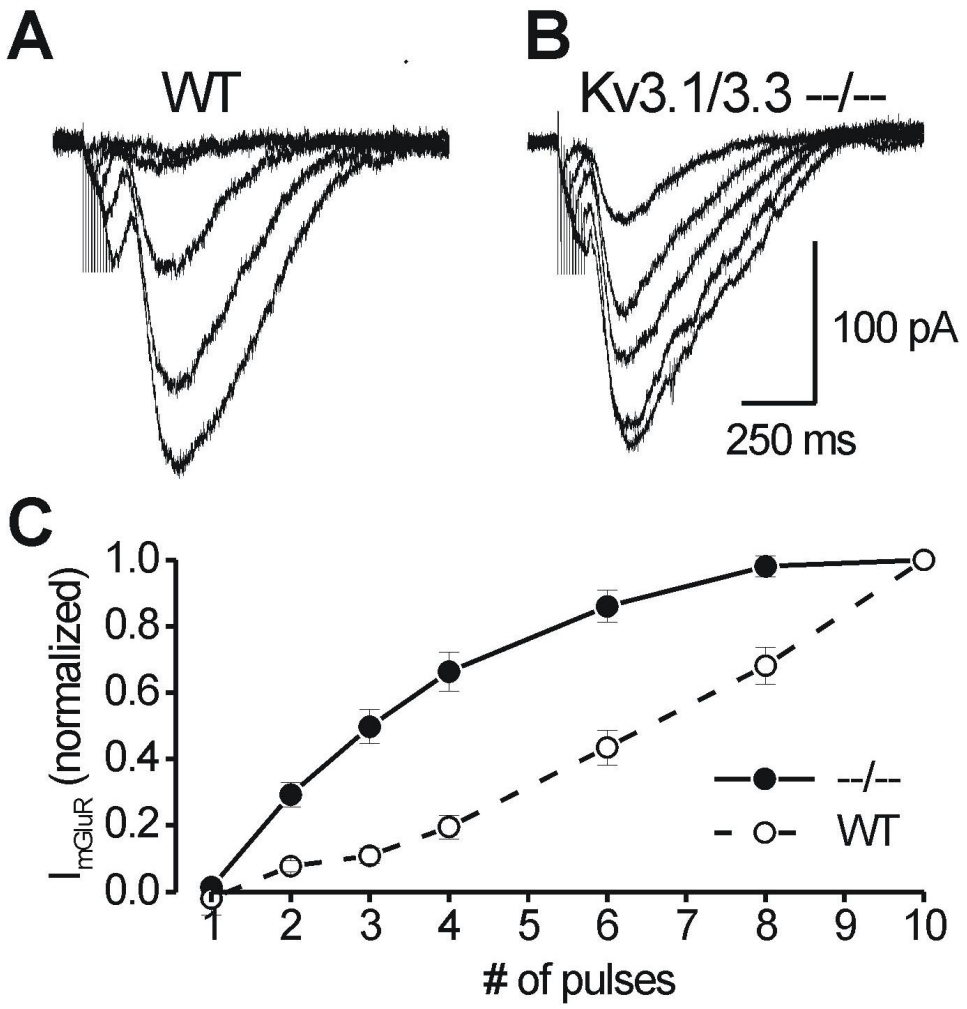

Figure 5.12: Potentiation of metabotropic glutamate receptor induced EPSC's. (A,B) Example traces of mGluR mediated EPSCs evoked by a train of 10,8,6,4 & 2 Pulses (10ms interval) in Purkinje cells of a WT and Kv3.1/3.3 -/- ,-/- mouse. (C) Relative response size versus train duration; each value is normalized to the mGluR EPSC evoked by a 10 stimuli train. Significantly larger fractional responses were observed in Kv3.1/3.3 DKO mice.

of mGluR-mediated currents is facilitated in Kv3.1/3.3 DKO mice, trains of stimuli were used to evoke mGluR-mediated EPSCs in WT and DKO mice (Fig. 5.12). Relative to the current induced with 10 pulses, mGluR mediated currents are clearly facilitated for smaller numbers of pulses in DKO mice, indicating that the increased release probability causes a much greater spillover of glutamate into the perisynaptic regions already (at a small number of pulses) compared to the WT.

In conclusion, increasing lack of Kv3 alleles translates into decreasing PPF, which is almost certainly due to increased release probability. Increased release probability also affects induction of mGluR - mediated potentials, which can be assumed to affect LTD induction in vivo and might be responsible for some of the phenotypic changes in mice lacking Kv3 alleles. It has been speculated that glutamate spillover might be highly regulated and that it could influence the adaptive behavior in an organism through LTD (Scanziani, 2002). All these changes seem to occur in an allele-dose dependent manner. High-sensitivity measurements of the ataxic phenotype in mice lacking Kv3 alleles showed an allele-dose dependent increase in ataxic gait, linking the observed changes at the cellular level of parallel fiber to Purkinje cell transmission to changes in behavior.

The explanation of the observed changes in PPF and mGluR-mediated EPSCs with the absence of Kv3 channels is quite straightforward knowing the prevailing function of Kv3 channels. The impairment in action potential conduction at high frequency (Fig. 5.9) is also similar to impairments in high-frequency firing observed in other cell types (for example see Wang et al.,1998). In contrast to the impairment in action potential conduction at high

frequency, which will reduce the dynamic range of granule cells at the upper end (see chapter 5.3), a high release probability can be assumed to reduce the dynamic range at the lower end, as a single action potential will already cause a large amount of glutamate to be released. This relatively large activation caused by a single action potential and the fact that a low number of activated synapses is sufficient to excite Purkinje cells (Barbour, 1993) could disturb the ability of the granule cell - Purkinje cell system to integrate and fine tune synaptic transmission in the massively converging system of granule cell – Purkinje cell signaling. Little is known about how the cerebellum performs its task and therefore it is difficult to argue which of the functional changes observed in Kv3 DKO mice are responsible for the observed phenotype, and several of the changes might act in concert to produce it.

The change in parallel fiber conduction velocity is not so easily explained and several changes could underlie an increased conduction velocity. Activity dependent changes in parallel fiber conduction velocity have been descried earlier (Gardner-Medwin, 1972), and some of the changes such as an increase in conduction velocity of subsequent action potentials in a train were replicated in this work (see next chapter). The next chapter describes a biophysical model of the granule cell axon (the parallel fiber) which explains these changes on a biophysical basis and will provide a better understanding of by which mechanisms Kv3 channels are expected to affect parallel fiber function.

6. Granule cell axon model

6.1 Simulation environment

Several models of cerebellar granule cells exist. They all model the granule cell soma, from which electrophysiology data is available. The most detailed models are constructed using the NEURON simulator (Hines and Carnevale, 1997). NEURON is a compartment-based neuron simulation environment and provides a powerful and flexible tool for implementing biologically realistic models of electrical and chemical signalling in neurons and networks of neurons. Another important feature of NEURON is its special facility for expanding and customizing its library of biophysical mechanisms such as voltage-gated ion channels, passive “leak” current and localized transmembrane shunts, ion accumulation, buffering, diffusion, and active transport. Furthermore there is ModelDB, a database for models of neurons, their cellular components (channels, synapses, etc.) and networks (Migliore et. al., 2002), from which previously published models can be conveniently downloaded. Mechanisms that are not yet implemented can be constructed using NMODL (short for Neuron MOdel Description Language), that describes a mechanism as a set of nonlinear algebraic equations, differential equations, or kinetic reaction schemes. The description employs a syntax that closely resembles familiar mathematical and chemical notation. The axon model described on the following pages was implemented in NEURON as described on the following pages.

6.2 Granule cell axon parameters

6.2.1 Dimensions

The granule cell axon is a simple structure. The axons, which make up the parallel fiber system, are unmyelinated axons running through the molecular layer. Due to their importance as a possible substrate of timing in the cerebellum, their structure has been described in relative detail. Since axonal diameter affects conduction velocity, a key variable in determining whether parallel fibers could function as a delay line, the distribution of axon diameter has been studied in detail in many species, including the mouse (Sultan, 2000). The mean diameter of mouse parallel fibers was 167 nm in the upper molecular layer, 180 nm in the middle molecular layer and 187 nm in the lower molecular layer, with a standard deviation of diameters between 44 and 48 nm (Sultan, 2000). The axon forms presynaptic boutons to contact one or more Purkinje cells or interneurons. These boutons have diameters up to about one micrometer. Approximately 20% of parallel fiber length is made up of such presynaptic boutons (Palay and Chan-Palay, 1974).

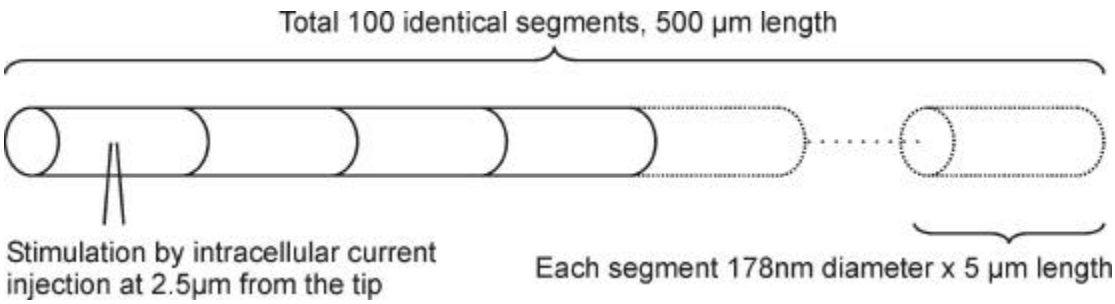

Fig. 6.1: Structure of the model granule axon.

Because of their significantly larger diameter, parallel fiber conduction velocity is largely determined by the axon (opposed to the bouton), where the initial depolarization will spread much slower. Fig. 6.1 shows the structure of the model granule cell. The axon diameter was set to 178nm, the mean axon diameter found in the mouse (Sultan, 2000). A length of 500µm and 100 segments were sufficient to record the relevant parameters of the model. Increasing the number of segments further did not significantly alter the predictions of the model.

6.2.2 Active membrane conductances

Sodium Channels

As in previous models, the fast sodium channel modeled by Gabbiani at al. (1994) from electrophysiological recordings from granule cells (Cull-Candy et al., 1989) was used. It assumes m^3h kinetics with voltage-dependent activation and inactivation variables m and h. In the absence of any electrophysiology data from granule cell axons, all sodium and potassium channel properties were adopted and densities (set via their maximum conductance) were set the same values as in Gabbiani et al. (1994).

Potassium channels

Cerebellar granule cells express Kv3.1, Kv3.3 and Kv3.4 (Weiser et. al., 1994; Rudy et al.,1999). These subunits assemble to form heteromultimeric channels of the delayed rectifier type and approximately correspond to the delayed rectifier channel in Gabbiani et al. (1994). Kv1.1 and Kv1.3 channels

were detected in parallel fibers using polyclonal antibodies (Veh et al., 1995; Chung et al., 2001), consistent with the expression of Kv1.1 and Kv1.3 mRNA in cerebellar granule cells (Kues and Wunder, 1992, Grigg et al., 2000). The hallmarks of this current are steady-state inactivation close to the resting membrane potential, large removal of inactivation with modest membrane hyperpolarizations (50% inactivation at –79 mV) and exponential inactivation following depolarization (Bardoni and Beluzzi, 1993). Also included was a small calcium-dependent potassium conductance that was found in the granule cell soma (Fagni et al., 1991). It's maximum conductance was ~12% of total maximum potassium conductance, but its contribution to the total potassium current during a single action potential elicited from the resting state was only 3%. It did not significantly affect action potential shape in WT even during trains of action potentials when calcium can reach a concentration several-fold of that at rest.

Neurons with brief spikes that use Kv3 channels to repolarize the action potential seem to have employed the strategy of using high channel densities (Rudy and McBain, 2001). The fast spiking interneurons in the neocortex and hippocampus have much larger potassium currents than pyramidal cells, the majority of which (> 75% in the neocortex) have Kv3-like properties (Erisier et al. ,1999, Martina et al., 1998, Hamill et al., 1991). Similarly, principal neurons in the medial nucleus of the trapezoid body have large potassium currents, of which the Kv3-like component accounts for more than 70% (Wang et al., 1998). The vast majority of potassium conductance was therefore assigned to the Kv3-like delayed rectifier potassium channel component, as in Gabbiani et al. (1994). The A-type and the calcium-

dependent potassium channel densities are also the same (A-type) or essentially the same (calcium-dependent conductance) as in D'Angelo et al. (2001).

Calcium channels and calcium extrusion

Resting Ca^{2+} concentrations within a presynaptic terminal are 50-100 nM and external Ca^{2+} levels are 2 mM, so there is an impressive gradient between internal and external Ca^{2+} concentrations. When an action potential invades a presynaptic bouton, it opens Ca^{2+} channels, giving rise to a locally high Ca^{2+} signal (10-100 µM) near open channels (Ca_{local}) (Chad and Eckert, 1984; Fogelson and Zucker, 1985; Simon and Llinas, 1985; Roberts et al., 1990; Matthews, 1996). As Ca^{2+} equilibrates throughout the bouton, a much smaller, long-lasting residual Ca^{2+} signal persists for tens of milliseconds to seconds (Ca_{res}), which, in contrast to Ca_{local}, can be readily measured with fluorescent Ca^{2+} indicators (Delaney et al. ,1989; Regehr and Atluri, 1995; Feller et al., 1996; Helmchen et al. , 1997; Ravin et al. ,1997).

Parameters affecting Ca^{2+} dynamics were adjusted to reproduce the results of Regehr and Atluri (1995), who measured bulk Ca^{2+} concentration changes in parallel fibers using fast and slow Ca^{2+} indicator dyes. The density of high-voltage activated potassium channels was adjusted so that a single action potential passing through the fiber leads to a Ca^{2+} transient with an amplitude of about 300 nM, which Regehr and Atluri deduced from the saturation of high affinity dyes. The density of the sodium-calcium exchanger was set to obtain a Ca^{2+} transient decay time constant of 150 ms, as measured in the same study. This study by Regehr and Atluri (1995) also

showed that for low affinity calcium indicators that faithfully reproduce the calcium transients, each stimulus in a 100 Hz train of 10 pulses produces the same change in fluorescence, i. e. the same change in intracellular Ca^{2+} concentration. This suggests that the dominant buffers in these terminals (if there are any) are low affinity, for, if they were high affinity, each successive stimulus in the train would produce successively larger increases in free calcium as the endogenous buffers become saturated. Since successive action potentials produced similar calcium transients, such a low affinity calcium buffer was not incorporated into the model since no data is available about the concentration of such buffers and their presence or absence would not affect any predictions or results gained from this model.

Previous models of granule cells (that did not include the axon) used several methods to model Ca^{2+} diffusion and buffering inside the soma. Equilibration of calcium concentration can take a significant amount of time inside the granule cell soma, which has a diameter of 5-10 µm. The characteristic time for equilibration is approximately $r^2/6D$ (Crank, 1975). With $D = 10^{-11}$ m^2/s and r = 89 nm for the axon, the equilibration time is less than 0.2 ms, sufficiently fast to neglect radial diffusion of Ca^{2+} in the axon (and treat radial diffusion as instantaneous). Since significant Ca^{2+} concentration gradients along the axon do not exist, axial diffusion of Ca^{2+} can be neglected. Similarly, intra-axonal diffusion of sodium and potassium, where gradients are even smaller than for Ca^{2+}, were also neglected.

6.2.3 Ion accumulation and passive leak conductances

In small, compact structures such as the bundles of granule cell axons traversing the molecular layer, significant changes in extra- and intracellular ion concentration can occur during high-frequency activation. Examples are extracellular potassium ion accumulation (Nicholson et al., 1977;Malenka et al.,1981), buildup of intracellular calcium concentration and intracellular sodium accumulation. In contrast to previous granule cell models, all intracellular ion concentrations were implemented as variables depending on the respective ionic currents. The sodium ion accumulation routine was adapted from the heart cell model from Courtemanche et al. (1998). Exchanging the ionic species from the sodium ion accumulation routine from Courtemanche et al. (1998) created potassium and calcium ion accumulation routines.

Changes in extracellular ion concentration are important only for potassium. The sodium ion concentration is large in the extracellular medium (140mM) and almost unchanged by activity. Extracellular calcium concentration in the cat cerebellum can exhibit activity-dependent changes (Nicholson et al.,1976), but only when postsynaptic structures are activated (Nicholson et al.,1978). Significant changes in extracellular potassium concentration have been shown to occur and affect parallel fiber excitability in response to repetitive stimulation of the molecular layer in cat (Nicholson et al.,1976; Nicholson et al.,1978) and rat (Nicholson et al.,1977;Malenka et al.,1981; Malenka and Kocsis, 1982) cerebellum *in vivo*. Pre- as well as postsynaptic activity contribute about equally to increase extracellular

Conductance	Ion	Gating type	Density	Density Unit	Reference
Fast sodium channel	Na^+	m^3h	70	$\frac{mS}{cm^2}$	Gabbiani et al.
Kv3 delayed rectifier potassium channel	K^+	m^4h	19	$\frac{mS}{cm^2}$	Gabbiani et al.
A-type potassium channel	K^+	m^3h	4	$\frac{mS}{cm^2}$	Gabbiani et al., D'Angelo et al.
Calcium-dependent potassium channel	K^+	o	3	$\frac{mS}{cm^2}$	Gabbiani et al., D'Angelo et al.
High-voltage-activated calcium channel	Ca^{2+}	m^2h	0.006	$\frac{mS}{cm^2}$	density modified, Gabbiani et al.
Sodium-Calcium Exchanger	Na^+/Ca^{2+}		$1 \cdot 10^{-9}$	$\frac{mA}{mM^4 \cdot cm^2}$	density modified, Gabbiani et al.
Sodium-Potassium Pump	Na^+ /K^+		1	$\frac{mA}{cm^2}$	Courtemanche et al., 1998
Sodium ion leak	Na^+		0.002	$\frac{mS}{cm^2}$	NEURON simulation environment
Potassium ion leak	K^+		0.002	$\frac{mS}{cm^2}$	NEURON simulation environment
Calcium ion leak	Ca^{2+}		$3 \cdot 10^{-6}$	$\frac{mS}{cm^2}$	NEURON simulation environment

Table 6.1: Ionic conductances contained in the granule cell axon membrane.

potassium concentration (Nicholson et al.,1978), and a single stimulation of a beam of parallel fibers can increase extracellular potassium concentration by as much as 0.5 mM (with both pre- and postsynaptic activation) (Malenka and Kocsis,1982). These concentration changes were measured using ion-selective micropipettes and it can be assumed that concentration changes in the tiny extracellular space between axons (see Fig.3.) are much larger. To calculate the amount of extracellular potassium concentration increase, the thickness of the extracellular space between the axons was assumed to be 30 nm and potassium concentration transients were assumed to decay with a time constant of 20 milliseconds.

Leak conductances for sodium, potassium and calcium and a sodium-potassium pump were inserted at densities that led a) to resting intracellular ion concentrations similar to those observe in slices *in vitro* and b) to a resting membrane potential of around –80mV as assumed by D'Angelo et al. (2001).

6.3 Limitations

The axon model does not contain many several receptors and signaling cascades that affect exocytosis. Most notably, glutamate receptors on the granule axon are neglected even though a variety of them are located in the presynaptic (i.e. parallel fiber) membrane and affects paired pulse facilitation (PPF). For example metabotropic glutamate receptor subtype 4 (Pekhletski et al.,1996), NMDA receptors (Casado et al., 2000) and kainate receptors (Delaney et al.,2002) are all found in the granule cell axon and have been shown to affect PPF. Parallel fiber NMDA receptor were shown to be activated

by action potentials in close succession and involved in LTD (Casado et al.,2002). But the dynamics of extracellular glutamate concentration, binding, clearance and the signaling mechanism how these receptors affect neurotransmitter release is largely unknown. Constructing a quantitative model of this activity-dependent feedback on the parallel fiber is not possible with the data currently available.

6.4 Results

At first, the most basic predictions of the model are compared with experimentally observed values, and the immediate effects of an absence of the Kv3 current in the model are compared with the experimentally observed differences between WT and DKO. As in other modeling studies investigating the contribution of Kv3 (Wang et al.,1998), the “virtual” WT is the granule cell axon as described, the Kv3.1 -/-,Kv3.3 +/- model is obtained by setting the Kv3 conductance to 25% of WT and the DKO model by setting the Kv3 conductance to zero.

6.4.1. Action potential width

Figure 6.2A shows the predicted action potential in “WT”, 25% Kv3 conductance and “DKO”. The action potential width predicted is shorter than the average measure in the experiment. This can be expected due to the low-pass filtering effect of the 2.7kHz sampling frequency optical recording system. The difference between model and experiment are smaller when one

looks at the differences in action potential width between the genotypes (Fig. 6.2C). Kv3 currents make up the vast majority of repolarizing potassium currents in the model (Fig. 6.2D). That the difference in action potential width observed experimentally is larger than the difference predicted by the model suggest that the density of the remaining potassium currents (A-type and calcium-dependent potassium current) in the axon could be lower than in the soma (where they were measured) or more generally, that the contribution of Kv3 to the repolarizing current could be even larger in reality than in the model. The model also predicts a large increase in calcium influx, 85% relative to the WT in the Kv3.1 -/-,Kv3.3 +/- model and 177% in the DKO model.

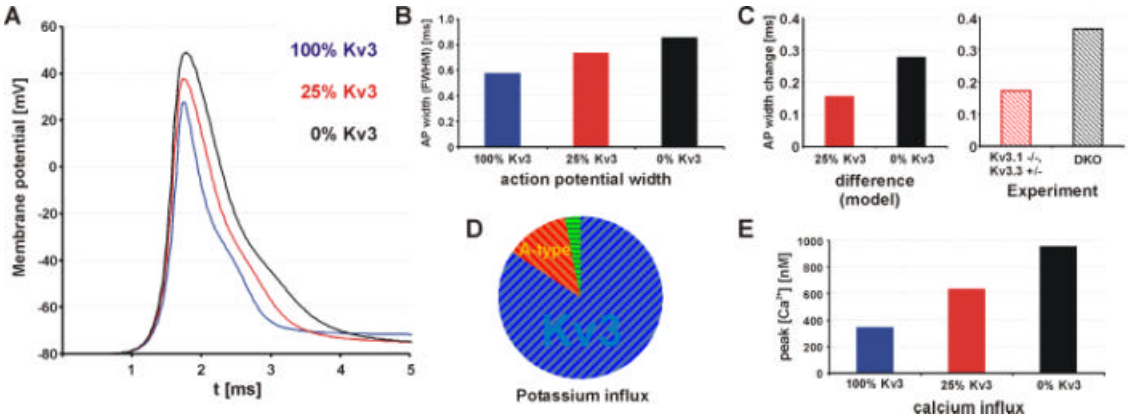

Fig.6.2: Action potential shape and calcium influx in the granule axon model. (A) Changes in the action potential shape induced by reducing Kv3 conductance (B) Action potential width for 100%Kv3 ("WT"): 0.58 ms, 25% Kv3: 0.737 ms, and 0% Kv3 ("DKO"): 0.86 ms. (C) AP broadening caused by reducing the Kv3 conductance to 25%: 0.157 ms; to zero: 0.28 ms, and comparison with the experimental result: 0.171 ms (Kv3.1 -/-, Kv3.3 +/-) and 0.363 ms (DKO). (D) Contribution of the three potassium channel species to the repolarizing current: Kv3 current 84.5%, A-type current 12.5%, Ca^{2+}-dependent current 3%. (E) Predicted Ca^{2+} influx / peak calcium concentration for "WT": 345 nM, for 25% Kv3: 638 nM and for no Kv3 ("DKO"): 954 nM.

Another interesting prediction that should be observed in the experiment too is an increase in action potential amplitude or peak voltage when Kv3 is reduced. Fluorescence signal amplitudes cannot be compared between WT and DKO experiments since the fluorescence signal cannot be connected to a certain change in membrane voltage. But a change in fluorescence signal caused by TEA with all other parameter kept constant (same slice, same location, same stimulation strength) can be compared between the genotypes. It is expected that the increase in fluorescence signals is largest in the WT (many TEA-sensitive channels), negligible in the DKO (few TEA-sensitive channels), and the Kv3.1 -/-, Kv3.3 +/- being in-between. Fig. 6.3A shows the change in action potential fluorescence signal amplitude induced by 1mM TEA to the bath together with the induced change in action potential width. On the basis of individual animals, AP amplitude is increased 28±4% in WT (mean±s.e.m., n=6), almost unchanged in Kv3.1 -/-, Kv3.3 +/- (0±8%, n=6) and slightly decreased in DKO (-7±3%, n=4).

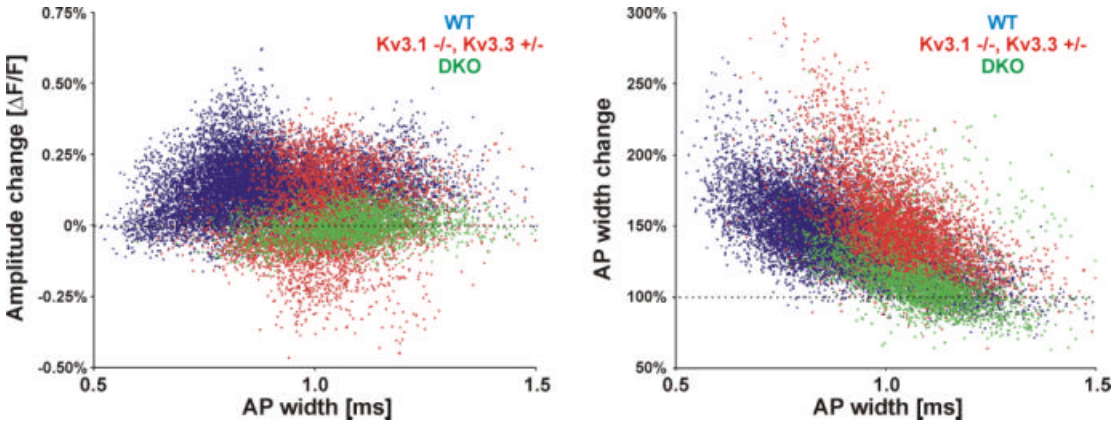

Fig. 6.3: Change in action potential amplitude (A) and action potential width (B) of individual data points induced by 1mM TEA, plotted against action potential width for WT(n=6 animals), Kv3.1 -/-, Kv3.3 +/- (n=6) and DKO (n=4). TEA has the least effect in the DKO, while AP amplitude as well as width is increased on average in the other genotypes.

This partly confirms the predictions of the model, i.e. that TEA should cause a larger increase in AP amplitude in the WT compared to the DKO. Contrary to expectation, TEA did not increase conduction velocity in all cases and the changes were not significant. The reduction in AP amplitude in the DKO suggests that other mechanisms cause a reduction in AP amplitude. This might most probably be phototoxicity of the voltage-sensitive dye, as phototoxicity can cause a gradual reduction in action potential amplitude in cultured neurons (Kuhn, 2001).

6.4.2 Action potential transmission capability at high frequency

The action potential conduction ability of the model axon in the presence (“WT”) and absence (“DKO”) of Kv3 is shown in Fig. 6.4. The observed effects are in very good agreement with the experimentally observed behavior. Stimulated at 100Hz, the model axon conducts action potentials also in the absence of Kv3, whereas stimulated at 200Hz, removing Kv3 causes a breakdown of action potential conduction after a few action stimulations. The model also replicates the decrease in compound action potential amplitude at 100Hz and even stronger at 200Hz (in the WT). The model predicts this decrease to be mainly due to activity-dependent buildup of extracellular potassium, which increases the potassium equilibrium potential. As a consequence, the ability of potassium channels to hyperpolarize the membrane is reduced, leading to a slightly depolarized “resting” state. The exact number of AP’s conducted in the absence of Kv3 at 200Hz depends on many factors such as resting membrane potential and the density of the

remaining potassium conductances. The gradual decline in amplitude of the voltage signal observed experimentally in the DKO at 200Hz can therefore be attributed to the inhomogeneity of parallel fibers, which will fail after an individually different number of AP's. This leads to the observed gradual decline in the measured compound action potential amplitude.

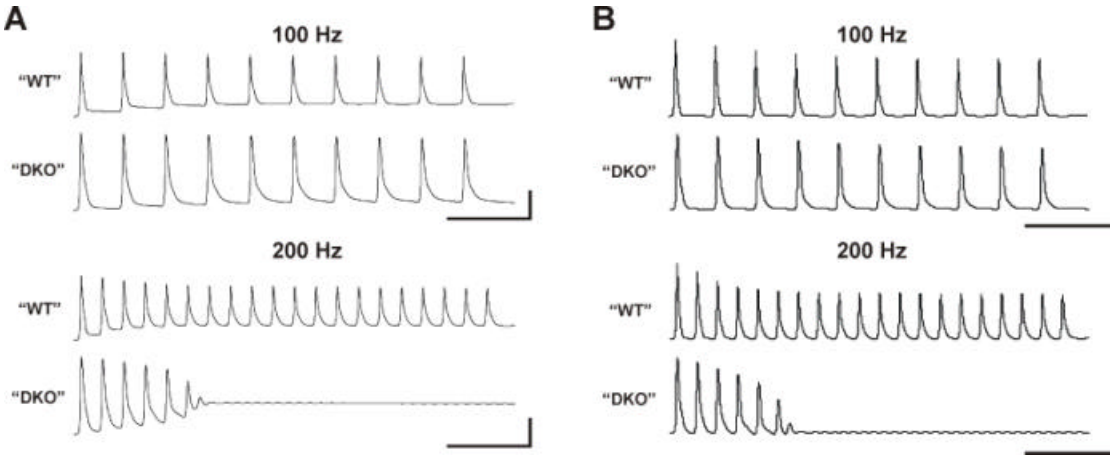

Fig. 6.4: High frequency action potential conduction. (A) shows the membrane potential in the model "DKO" and "WT" axon in response to 10 and 20 stimuli at 100Hz and 200Hz. To facilitate comparison with the voltage signal recorded experimentally (Fig. 5.9), (B) shows the membrane potential after the same high-pass filtering and normalization to the first action potential as in the experimental data. Scale bars are 20ms and 50mV.

6.4.3 Conduction velocity

Figure 6.5 shows the three most important parameters that affect parallel fiber conduction velocity. Increasing the axon diameter as well as increasing the resting membrane potential causes the action potential to propagate faster. Surprising at first, changing the density of the Kv3 current also significantly affects conduction velocity. While this effect was unexpected, the mechanism

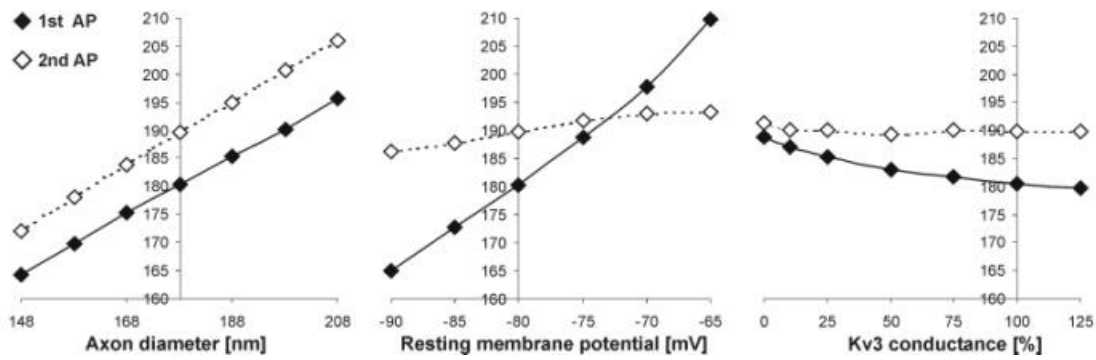

Fig. 6.5: Axon parameters affecting the conduction velocity of a first and 10ms delayed second parallel fiber action potential. The y-axis shows the conduction velocity in mm/s and is positioned at the standard value of axon diameter, resting membrane potential and Kv3 conductance.

becomes clear after looking at how action potentials propagate. To understand how action potentials propagate, one must consider *local potentials*, which are subthreshold changes in membrane potential. Local potentials do not propagate, but decay with distance from their origin; if sufficiently large, they initiate an action potential. To understand the behavior of local potentials, the axonal membrane is considered passive. The passive membrane properties are the properties of the membrane at resting potential. If the membrane becomes depolarized to a certain voltage somewhere, the local potential will exponentially decay from this voltage to the resting membrane potential with a length constant λ. The length constant λ depends on the axonal geometry, according to (Sargent, 1992; Rall, 1995):

$$l = \sqrt{\frac{R_m}{R_i + R_o}},$$

where R_m is the passive membrane resistance of each annular segment, R_i is the internal axial resistance and R_o is the axial resistance of the external

medium. For small unmyelinated axons, λ is in the order of 100 µm (Sargent, 1992). R_o is often ignored since it is negligible compared to R_i in many cases.

Once the local potential increases past the spike initiation threshold (around –40 mV), an action potential is initiated. The action potential propagates via the passive mechanism of local potentials and conduction velocity is proportional to the length constant λ. Other factors that affect membrane conduction velocity are the axonal membrane capacitance, the sodium and potassium channel densities and their activation kinetics.

Both R_m and R_i are altered by changing the diameter of the axon. Doubling the diameter results in a twofold decrease in R_m, since there is twice as much membrane and twice as many channels per unit length (assuming that channel density remains constant). Doubling the diameter causes a fourfold decrease in R_i, however, because the cross-sectional area of the axon is increased by a factor of four. Therefore, doubling the diameter increases λ and, if R_o is can be neglected, causes a $\sqrt{2}$-fold increase in conduction velocity.

Figure 6.6 illustrates how the three factors axon diameter, resting membrane potential affecting and (density of the) Kv3 current affect action potential conduction velocity. Increasing axon diameter will increase the length constant λ. Increasing resting membrane potential will reduce the increase in local potential necessary to reach spike threshold. Reducing the density of Kv3 channels will increase the action potential amplitude and therefore the voltage from which the local potential will decay, causing the axon to reach threshold “further away”.

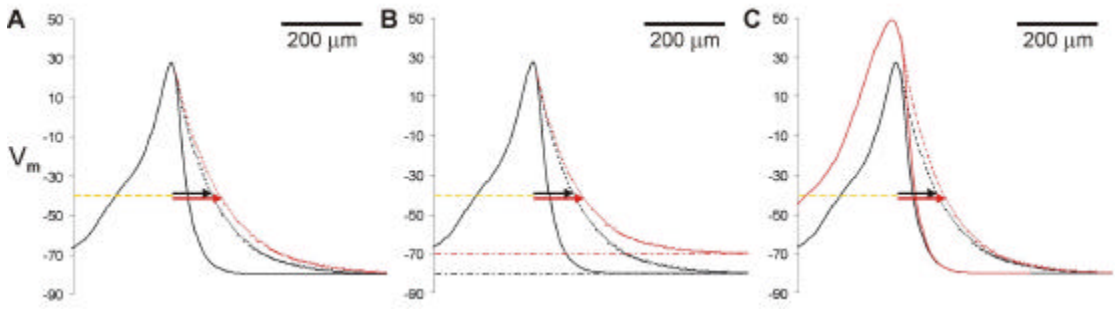

Fig. 6.6: Action potential propagation via local potentials. The figure shows membrane potential as a function of space and how it would decay from a depolarization if the membrane were passive and the membrane potential $V_m(x)$ static (dashed black and red lines). The action potential propagates to the right. A dashed yellow line marks the spike initiation threshold (at –40 mV). How far the passive spread of membrane potential would depolarize the membrane above threshold (red and black arrows) determines conduction velocity. The conduction velocity can be increased by (A) increasing the axon diameter or (B) increasing the resting membrane potential to –70 mV from -80 mV. (C) In the Kv3 DKO model, the conduction velocity is increased due to a larger action potential (using the action potential shapes of "WT"(black) and "DKO"(red) shown in Figure 6.2).

The model also predicts that a second action potential delayed 10 ms would travel about 5% faster under standard conditions (marked by the conduction velocity axis in Figure 6.5). Such an increase was observed previously (Gardner-Medwin, 1972; Malenka et al.,1981; Kocsis et al.,1983), but also in the experiments of this work. In WT, the conduction velocity increase for a second action potential volley delayed 10 ms lies between 8% and 29%, on average 15% (n=5). If the model would incorporate all factors that could affect conduction velocity, the higher increase found experimentally suggests that the granule axon resting membrane potential might be even lower or the extracellular potassium transients even bigger than assumed in the model.

6.4.4 Homogeneity of parallel fiber conduction velocity

Granule axons of several species have been found to exhibit a gradient in their diameter across the molecular layer, with superficial axons being thinner than deeper axons close to the Purkinje cell layer. In the mouse, the difference in the mean diameter of parallel fibers between the upper and lower third of the molecular layer has been found to be 20 nm (Sultan, 2000). As conduction velocity depends on fiber diameter, deeper axons would therefore be expected to conduct action potentials faster. Depth-dependent differences in conduction velocity have been found in frontal slices of rat cerebellar cortex using a similar voltage-sensitive dye recording technique (Vranesic et al., 1994). The homogeneity of parallel fiber conduction velocity is a critical parameter in several theories on how the cerebellum works. Two opposing views have received widespread attention, one arguing that the slow and well-organized conduction velocity enables the parallel fiber-Purkinje cell system to de- and encode temporal patterns (Braitenberg, 1983 & 1987; Heck, 1993; Braitenberg et al., 1997; Braitenberg, 2002). The other is based on an apparently strong ascending granule cell axon synapse (Gundappa-Sulur et al.,1999) causing “patchy” activation (Cohen & Yarom 1998), weak parallel fiber synapse (Cohen & Yarom, 1998), and the apparent absence of correlation in the firing in neighboring Purkinje cells in the direction of parallel fibers *in vivo* (Bower & Woolston, 1983).

Judging from the broadness of the activated region of parallel fibers (for example see Fig. 5.3), the diameter of the parallel fiber bundle activated by

extracellular stimulation seems to be about 100 micrometers. Assuming the diameter of activated parallel fiber bundle is the same in the depth direction of the molecular layer and the thickness of the molecular layer in this lobule of the cerebellar cortex is 150 micrometers, the mean parallel fiber thickness in the activated bundle of fibers differs by 20 nm. Using the influence of parallel fiber diameter on conduction velocity found in the model, this would translate into 10 mm/s difference in conduction velocity between fibers of the lower and upper edge of the activated bundle, or about 5% of the mean WT conduction velocity of 184 mm/s. This would shift the upper and lower action potential 0.27 ms relative to each other (per mm traveled), which would cause a broadening of the compound action potential of about 0.2 ms (per mm traveled for a WT action potential, calculation not shown). Figure 6.7 shows the experimentally observed broadening of the compound action potential that consists of individual action potentials propagating in individual granule cell axons. As can be seen from the histogram, the range of

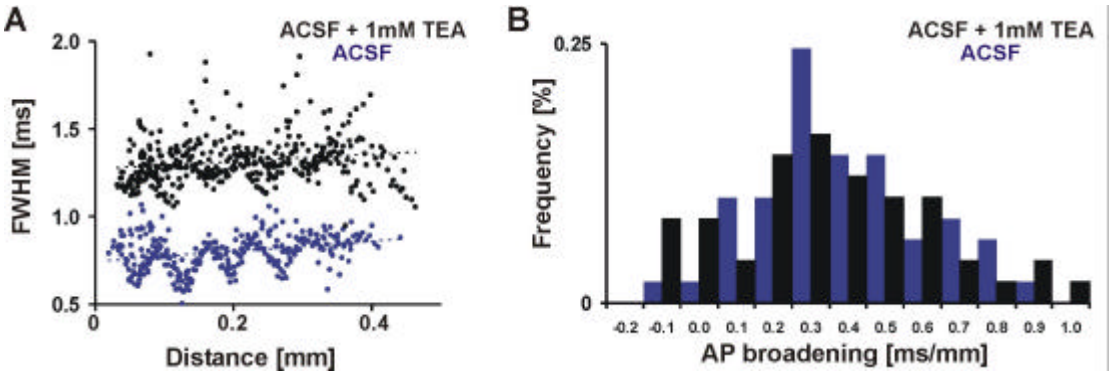

Fig. 6.7: Broadening of the Compound action potential. (A) The compund action potential gradually broadens as it travels away from the stimulation site (Example WT) (B) Histogram of the amount of broadening observed in normal ACSF and in the presence of TEA. The range of broadening observed was similar. The broadening expected from the anatomy is about 0.2 ms/mm.

broadening observed was quite large. No significant difference was observed between WT and DKO. The effect of adding TEA was non-uniform. Furthermore, the amount of broadening did not systematically depend on whether the propagating action potential was part of a train, its frequency or the position of the propagating volley within a train of action potentials.

In conclusion, it can be said that the amount of broadening expected from the anatomical gradient in parallel fiber diameter lies well within the observed range. A relatively large range of broadening at times observed in the same slice suggests that inhomogeneities in parallel fiber diameter are not the only cause of broadening and that several other sources of error cause broadening of the voltage-sensitive dye signal. Nevertheless, the amount of broadening is small enough to support the parallel fiber timing hypothesis of cerebellar function.

6.4.5 Conduction velocity and on-beam hyperpolarization

On-beam hyperpolarization is the phenomenon of an apparent hyperpolarization of the region coincident with the activated beam of parallel fibers. In contrast to previous findings (Cohen et al., 2000), the hyperpolarization observed in this work was not affected by blocking synaptic transmission. The excellent coincidence with the activated parallel fiber bundle (see Fig. 3.4 for an example) leads to the impression that on-beam hyperpolarization is a hyperpolarization of parallel fibers. This theory can be tested using the predictions of the axon model. A hyperpolarization of parallel

fibers should slow down the action potential. Since on-beam hyperpolarization is observed when a train of stimuli activates parallel fibers, the stimulus should propagate slower when the parallel fiber is hyperpolarized. As Figure 6.8 demonstrates, this is NOT the case. Parallel fiber conduction velocity increases from the first to the second pulse as predicted by the model mainly due to accumulation of extracellular potassium (Kocsis et al., 1983; Malenka et al., 1983), but conduction velocity is not reduced as on-beam

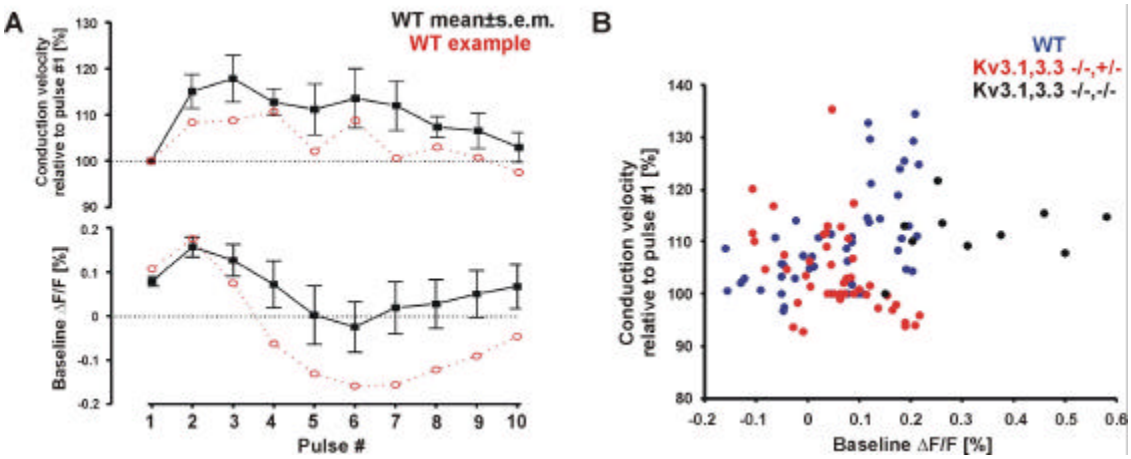

Fig. 6.8: On-beam hyperpolarization (reflected in baseline fluorescence change) does not affect conduction velocity. (A) 100Hz trains of action potentials hyperpolarize the baseline, but do not slow the action potential. After the first pulse, the baseline is increased by about 0.15% and conduction velocity by approximately 15% (average of n=5 animals). Reversal of the baseline to a negative fluorescence at pulse 5 to 6 is not accompanied by a significant reduction in conduction velocity. (B) Action potential conduction velocity during 100 Hz trains is not correlated with changes in baseline fluorescence for any genotype (data from 12 animals).

hyperpolarization appears. Conduction velocity stays increased relative to the first pulse even as the region of activated parallel fibers is (apparently) hyperpolarized. This suggest that the phenomenon of on-beam

hyperpolarization is not due to a hyperpolarization of the parallel fiber cell membrane. Possible origins of the signal include the hyperpolarization of other structures co-located with the parallel fiber beam. Another possibility is a contribution of an activity-dependent intrinsic fluorescence signal from mitochondrial flavoproteins that become oxidized in response to metabolic activation of the parallel fiber mitochondria (Reinert et al., 2002).

7. Conclusions

Optical Imaging

The present work demonstrates a new range of sophisticated analytical methods that can be applied to optical imaging data. A state-of-the-art back-illuminated CCD camera offers much better resolution and sensitivity than techniques used previously to image cerebellar circuit dynamics. Phenomena such as lateral inhibition and on-beam hyperpolarization were visualized at previously unachieved resolution. Sophisticated programs for the automated analysis of individual pixel data allow for advanced analytical capabilities such as setting a threshold for significant signal size, detecting the origin of the stimulus, measuring conduction velocities and a variety of other parameters that are difficult and time-consuming to analyze manually. Together with the systematic variation of other parameters such as for example stimulus frequency, the extracellular solution composition and the animal genotype, optical imaging allows analyzing the interaction and interdependence of many factors. Besides saving a lot of time, automated analysis can also produce intuitive figures such as the maps of action potential width that are impossible to produce manually. The measurement of conduction velocity in single slices is very precise (the median correlation coefficient between distance and rise time point was 0.993) and opens up the possibility to use conduction velocity as a sensitive indicator of factors that affect axon physiology.

Granule axon model

The granule axon model was constructed straightforward from previous models of the granule cell soma. Even though many parameters in the axon are unknown, using values from previous models (where they can also differ several-fold between different models) resulted in predictions that were in surprisingly good agreement with the experiments. It should be emphasized that little attempts were made here to optimize the “fit” of the model to the data. The biggest strength of the model is the mechanistic explanation of the phenomena observed, even if the predicted values are not in perfect agreement. In light of the many shortcomings and simplifications incorporated into the model, adjusting conductances and concentrations to a “perfect” fit will not result in a credible and solid prediction of quantitative aspects of the granule cell axon such as for example the density of a certain ion channel.

The power of the granule axon model is illustrated here in the convincing rebuttal of the theory that on-beam hyperpolarization is a hyperpolarization of the parallel fiber membrane. Looking at the optical imaging data only, the perfect co-location of activated parallel fiber beam and on-beam hyperpolarization is very convincing in favor of this hypothesis. But the granule axon model predicts that hyperpolarization would lead to a slowing of the action potential, a thing that is never observed in the experiment. The model provides a powerful and solid justification that this hypothesis is false. The exact nature of the on-beam hyperpolarization remains a mystery.

Neurobiology

This work demonstrates the important role of Kv3 potassium channels in regulating action potential shape and synaptic transmission. From a systems biology point of view, too little is known about how the cerebellum works to determine which of the observed changes in the properties of parallel fibers are responsible for which phenotype. An important finding is the alteration in the induction of metabotropic glutamate receptor-mediated potentials. This shows that the absence of Kv3 channels should have a strong effect on cerebellar plasticity, a phenomenon that, in contrast to alterations in release probability and short term plasticity, is well understood from studying the phenotype of mice lacking metabotropic glutamate receptors and other downstream components of the plasticity signaling pathway. How the gradual broadening of the action potential and the concomitant changes in release probability and short-term plasticity contribute to the phenotype is open to speculation. Very interestingly though, mice lacking both alleles of Kv3.1 and one allele of Kv3.1 exhibit a discernible ataxic gait, but none of the other phenotypic changes in Kv3.1/3.3 double-knockout mice. Measurements using a highly sensitive movement detection system demonstrated a gradual increase in a measure of ataxia with an increasing lack of Kv3.1 and Kv3.3 alleles (Matsukawa et al., 2003). These allele-dose dependent changes suggest that Kv3 channels play a causal role in the observed ataxia, but through which of the above mechanism is unclear. Interestingly, mice that lack the mGluR4 metabotropic glutamate receptor or the Munc13 synaptic protein

show an alteration in paired-pulse facilitation as well as motor performance deficits (Augustin et al.,2001; Pekhletski et al., 1996). This points towards the possibility that normal short-term plasticity might also be necessary for normal cerebellar function.

Secondly, this work upholds parallel fiber conduction delay as a possible substrate of timing in the cerebellar cortex since the divergence of conduction velocity is small. Parallel fiber conduction velocity can be affected, maybe even adjusted through varying ion channel densities or functional properties via changes in expression or functional state such as phosphorylation. It seems that conduction velocity is quite homogeneous across fibers in the upper and lower regions of the molecular layer, as would be expected from the small difference in their diameters in mouse cerebellum. That such an elaborate system (anatomical as well as functional) has evolved and that obviously a great effort is made to keep this system against evolutionary pressure, is a strong argument that the parallel fiber system and possibly the delay carried by its conduction velocity is important to cerebellar function. Nitric oxide plays an important role in the induction of synaptic plasticity at the parallel fiber – Purkinje cells synapse (Daniel et. al., 1998, Ito, 2000). It has been shown that Kv3.1 channel conductance can be suppressed by NO, an effect that appears to be mediated by the activation of a serine-threonine phosphatase such as PP2A (Moreno et. al., 2001). PP2A is expressed in cerebellar granule cells (Abe et. al., 1994). Moreover, casein kinase 2, an ubiquitous second messenger-independent serine-threonine protein kinase

believed to be constitutively active, determines the voltage-dependence of the Kv3.1 channel (Macica and Kaczmarek, 2001). Therefore, a complete set of protein kinase and phosphatase is present in the granule cell axon, permitting regulation of Kv3.1-mediated potassium currents through phosphorylation and dephosphorylation. Dephosphorylation of Kv3.1 in neurons of the medial nucleus of the trapezoid body with inhibitors of casein kinase 2 rendered them unable to follow high frequency stimuli (Macica and Kaczmarek, 2001). The immediate effects of altering Kv3.1 conductance demonstrated in this work suggest a possibly important way of modulating synaptic transmission at the parallel fiber – Purkinje cell synapse.

This work demonstrates the power of optical imaging in answering questions that cannot be addressed using other techniques. This is especially true for the cerebellar cortex, whose characteristic anatomy simplifies the interpretation of optical signals. Several questions remain and can be investigated using the methods developed in this work, such as for example the origin of on-beam hyperpolarization and whether second messengers such as NO can also influence conduction velocity.

REFERENCES

Abe H, Shima H, Sekiguchi M, Guo H, Nagao M, Tamura S, Kondo H (1994) Localization of mRNA for protein phosphatase 2A in the brain of adult rats. Mol. Brain Res. 22:139-143

Aiba A, Kano M, Chen C, Stanton ME, Fox GD, Herrup K, Zwingman TA, Tonegawa S (1994) Deficient cerebellar long-term depression and impaired motor learning in mGluR1 deficient mice. Cell 79:377-388

Albus JS (1971) A theory of cerebellar function. Math. Biosci. 10:25-61

Andersen BB, Korbo L, Pakkenberg G (1992) A quantitative study of the human cerebellum with unbiased stereological techniques. J Comp. Neurol. 326:549-560

Atluri PP, Regehr WG (1996) Determinants of the time course of facilitation at the granule cell to Purkinje cell synapse. J Neurosci 16:5661-5671.

Augustine GJ (1990) Regulation of transmitter release at the squid giant synapse by presynaptic delayed rectifier potassium current. J. Physiol. (Lond) 431:343-364.

Augustine I, Korte S, Rickmann M, Kretzschmar HA, Sudhof TC, Herms JW, Brose N (2001) The cerebellum-specific Munc13 isoform Munc13-3 regulates cerebellar synaptic transmission and motor learning in mice. J Neurosci 21:10-17.

Barbour B (1993) Synaptic Currents Evoked in Purkinje Cells by Stimulating Individual Granule Cells. Neuron 11:759-769.

Bardoni R, Belluzzi O (1993) Kinetic study and numerical reconstruction of A-type current in granule cells of rat cerebellar slices. J Neurophysiol. 69:2222-2231

Batchelor AM, Madge DJ, Garthwaite J (1994) Synaptic activation of metabotropic glutamate receptors in the parallel fibre – Purkinje cell pathway in rat cerebellar slices. Neuroscience 63:911-915

Batchelor AM, Garthwaite J (1997) Frequency detection and temporally dispersed synaptic signal association through a metabotropic glutamate receptor pathway. Nature 385:74-77

Batchelor AM, Knöpfel T, Gasparini F, Garthwaite J (1997) Pharmacological characterization of synaptic transmission through mGluRs in rat cerebellar slices. Neuropharmacology 36:401-403

Baude A, Nusser Z, Robert JD, Mulvihill E, McIlhinney RA, Somogyi P (1993) The metabotropic glutamate receptor (mGluR1 alpha) is concentrated at perisynaptic membrane of neuronal subpopulations as detected by immunogold reaction. Neuron 11:771-787

Bower J, Woolston DC (1983) Congruence of spatial organization of tactile projections to granule cell and Purkinje cell layers of cerebellar hemispheres of the albino rat: vertical organization of cerebellar cortex. J. Neurophysiol. 49:745-766.

Bower J (2002) Parallel Fiber Beams: What Do They Do ? Ann. N.Y. Acad. Sci. 978:184-187

Braitenberg V, Atwood RP (1958) Morphological observations on the cerebellar cortex. J. Comp. Neurol. 109:1-33

Braitenberg V (1983) The cerebellum revisited. J. Theoret. Neurobiol. 2:237-241

Braitenberg V (1987) in Glickstein et al. (Eds.), Cerebellum and Neuronal Plasticity, Plenum, 1987, pp. 193-207

Braitenberg V,Heck D, Sultan F (1997) The detection and generation of sequences as a key to cerebellar function: experiments and theory Behav. Brain Sci. 20:229-277.

Braitenberg V (2002) In defense of the cerebellum. Ann. N.Y. Acad. Sci. 978:175-183

Bravin M, Morando L, Vercelli A, Rossi F, Strata P (1999) Control of spine formation by electrical activity in the adult rat cerebellum. Proc. Nat. Acad. Sci. 96:1704-9

Brew HM, Forsythe ID (1995) Two voltage-dependent K^+ conductances with complementary functions in postsynaptic integration at a central auditory synapse. J Neurosci 15:8011-8022.

Carter AG, Regehr WG (2000) Prolonged Synaptic Currents and Glutamate Spillover at the Parallel Fiber to Stellate Cell Synapse. J. Neurosci. 20(12):4423-4434.

Casado M, Dieudonne S, Ascher P. (2000) Presynaptic N-methyl-D-aspartate receptors at the parallel fiber-Purkinje cell synapse. Proc. Nat. Acad. Sci. 97(21):11593-11597.

Casado M, Isope P, Ascher P (2002) Involvement of presynaptic N-methyl-D-aspartate receptors in cerebellar long-term depression. Neuron 33(1):123-30.

Celio MR, Baier W, de Viragh P, Gregersen HJ, Norman AW, Schärer L (1989) Cell Calcium 11:599-602.

Chad JE, Eckert R (1984) Calcium domains associated with individual channels can account for anomalous voltage relations of Ca-dependent responses. Biophys. J. 45:993-999.

Chan E (1997) Regulation and function of Kv3.3. PhD thesis, The Rockefeller University.

Chung YH, Shin C, Kim MJ, Lee BK, Cha CI (2001) Immunohistochemical study on the distribution of six members of the Kv1 channel subunits in the rat cerebellum. Brain Res. 895:173-177

Coetzee WA, Amarillo Y, Chiu J, Chow A, Lau D, McCormack T, Moreno M, Nadal MS, Ozaita A, Pountney D, Saganich M, Vega-Saenz de Miera E, Rudy B (1999) Molecular Diversity of K^+ Channels. Ann. New York Acad. Sci. 868:233-285

Cohen D, Yarom Y (1998) Patches of synchronized activity in the cerebellar cortex evoked by mossy-fiber stimulation: Questioning the role of parallel fibers. Proc. Nat. Acad. Sci. 95:15032-15036

Cohen D, Yarom Y (2000) Cerebellar on-beam and lateral inhibition: two functionally distinct circuits. J Neurophysiol 83(4):1932-40

Conquet F, Bashir ZI, Davies CH, Daniel H, Ferraguti F, Bordi F, Franz-Bacon K, Reggiani A, Matarese V, Conde F (1994) Motor deficit and impairment of synaptic plasticity in mice lacking mGluR1. Nature 372:237-243

Covarrubias M, et. al. (1994) Elimination of rapid potassium channel inactivation by phosphorylation of the inactivation gate. Neuron 13:1403-1412.

Crank J (1975) The Mathematics of Diffusion, 2nd Edition. Clarendon Press, Oxford.

Cull-Candy SG, Marshall CG, Ogden D (1989) Voltage-activated membrane currents in rat cerebellar granule neurons. J Physiol. Lond. 414:179-199.

Delaney AJ, Jahr CE (2002) Kainate receptors differentially regulate release at two parallel fiber synapses. Neuron 36(3):475-82

Delaney KR, Zucker RS, Tank DW (1989) Calcium in motor nerve terminals associated with posttetanic potentiation. J. Neurosci. 9:3558-3567

Dittman JS, Kreitzer AC, Regehr WG (2000) Interplay between Facilitation, Depression, and Residual Calcium at Three Presynaptic Terminals. J. Neurosci. 20(4):1374-1385.

Drejer J, Larsson OM, Schousboe A (1983) Characterization of uptake and release processes for D- and L-aspartate in primary cultures of astrocytes and cerebellar granule cells. Neurochem Res. 8(2):231-43.

Ebner TJ, Chen G (1995) Use of Voltage-sensitive Dyes and Optical Recordings in the Central Nervous System. Progress in Neurobiology 46:463-506.

Eccles JC, Ito M, Szentagothai J (1967) The cerebellum as a Neuronal Machine, Springer Verlag, Berlin

Edwards FA, Konnerth A, Sakmann B, Takahashi T (1989) A thin slice preparation for patch clamp recording from neurones of the mammalian central nervous system. Pflügers Arch 414:600-612

Erisir A, Lau D, Rudy B, Leonard CS. (1999) Function of specific K(+) channels in sustained high-frequency firing of fast-spiking neocortical interneurons. J. Neurophysiol. 82(5):2476-89.

Espinosa F, McMahon A, Chan E, Wang S, Ho CS, Heintz N, Joho RH (2001) Alcohol hypersensitivity, increased locomotion, and spontaneous myoclonus in mice lacking the potassium channels Kv3.1 and Kv3.3. J. Neurosci. 21(17):6657-65.

Fagni L, Bossu JL, Bockaert J (1991) Activation of a large Ca2+-dependent K+ channel by stimulation of glutamate phosphoinositide-coupled receptors in cultured cerebellar granule cells. Eur. J. Neuroscience 3:778-789.

Feller MB, Delaney KR, Tank DW (1996) Presynaptic calcium dynamics at the frog retinotectal synapse. J. Neurophysiol. 76:381-400.

Finch EA, Augustine GJ (1998) Local calcium signaling by inositol-1,4,5-triphosphate in Purkinje cell dendrites. Nature 396:753-756

Fogelson AL, Zucker RS (1985) Presynaptic calcium diffusion from various array of single channels. Implications for transmitter release and synaptic facilitation. Biophys. J. 48:1003-1017.

Fox DA, Ruan D (1989) Time- and frequency-dependent effects of potassium channel blockers on large and medium diameter optic tract axons. Brain Research 498:229-242.

Gabbiani F., Midtgaard J. and Knöpfel T. (1994) Synaptic integration in a model of cerebellar granule cells. J. Neurophysiol. 72:999-1009.

Gall D, Susa I, D'Angelo E, Rossi P, Schurmanns S, Schiffmann SN (2001) Altered Electroresponsiveness of Cerebellar Granule Cells in Mice Lacking Calretinin. *2001 Abstract Viewer/Itinerary Planner.* Washington, DC: Society for Neuroscience

Garcia-Segura LM, Baetens D, Roth J, Norman AW, Orci L (1984) Brain Research 296:75-86.

Gardner-Medwin AR (1972) An extreme supernormal period on cerebellar parallel fibers. J. Physiol. 222:357-371.

Geiger JRP, Jonas P (2000) Dynamic Control of Presynaptic Ca2+ Inflow by Fast-Inactivating K^+ Channels in Hippocampal Mossy Fiber Boutons. Neuron 28:927-939.

Grigg JJ, Brew HM, Tempel BL. (2000) Differential expression of voltage-gated potassium channel genes in auditory nuclei of the mouse brainstem. Hear Res 140(1-2):77-90.

Gundappa-Sulur G, De Schutter E, Bower J (1999) Ascending Granule Cell Axon: An important Component of Cerebellar Cortical Circuitry. J. Comparative Neurology 408:580-596

Hamill OP, Marty A, Neher E, Sakmann B, Sigworth FJ (1981) Improved patch clamp techniques for high-resolution current recording from cells and cell free patches. Pflügers Arch 391:85-100

Hamill OP, et. al. (1991) Patch-clamp studies of voltage-gated currents in identified neurons of the cerebral cortex. Cereb. Cortex 1:48-61

Heck D (1993) Rat cerebellar cortex in vitro responds specifically to moving stimuli. Neurosci Lett. 157(1):95-8.

Helmchen F, Borst JGG, Sakmann B (1997) Calcium dynamics associated with a single action potential in a CNS presynaptic terminal. Biophys. J. 72:1458-1471

Hines ML, Carnevale NT (1997) The NEURON Simulation Environment. Neural Computation 9:1179-1209.

Hirano T, Hagiwara S (1988) Synaptic transmission between rat cerebellar granule cells and Purkinje cells in dissociated cell culture: effects of excitatory-amino acid transmitter antagonists. Proc. Nat. Acad. Sci. 85:934-938.

Ho CS, Grange RW, Joho RH. (1997) Pleiotropic effects of a disrupted K+ channel gene: reduced body weight, impaired motor skill and muscle contraction, but no seizures. Proc. Natl. Acad. Sci. USA 94(4):1533-38.

Hodgkin AL, Huxley AF (1952) A quantitative description of membrane current and its application to conduction and excitation in nerve. J. Physiol. 117: 500-544.

Ichise T, Kano M, Hashimoto K, Yanagihara D, Nakao K, Shigemoto R, Katsuki M, Aiba A (2000) mGluR1 in cerebellar Purkinje cells essential for long-term depression, synapse elimination, and motor coordination. Science 288:1832-1835

Ito M (2000) Mechanisms of motor learning in the cerebellum. Brain Research 886(1-2):237-245.

Ito M (2002) Historical review of the significance of the cerebellum and the role of Purkinje cells in motor learning. Ann N Y Acad Sci. 978:273-88.

Iwasato T, Datwani A, Wolf AM, Nishiyama H, Taguchi Y, Tonegawa S, Knopfel T, Erzurumlu RS, Itohara S. (2000) Cortex-restricted disruption of NMDAR1 impairs neuronal patterns in the barrel cortex. Nature 406(6797):726-31.

Joho RH, Ho CS, Armitage R, Marks G (1997) Physiological and behavioral alterations in a mutant mouse deficient for the voltage-gated K^+ channel Kv3.1. Pflügers Arch 434:R90-R91

Joho RH, Ho CS, Marks GA (1999) Increased γ- and decreased δ-oscillations in a mouse deficient for a potassium channel expressed in fast-spiking interneurons. J Neurophysiol. 82:1855-1864.

Jourdon P, Berwald-Netter Y, Dubois JM (1986) Effects of dimethylsulfoxide on membrane currents of neuroblastoma x glioma hybrid cell. Biochimica et Biophysica Acta 856:399-402

Jorntell H, Ekerot C (2003) Mossy fiber synaptic input to cerebellar granule cells *in vivo*. 2003 Abstract Viewer/Itinerary Planner. Washington, DC: Society for Neuroscience

Kase M, Miller DC, Noda H. (1980) Discharge of Purkinje cells and mossy fibers in the cerebellar vermis of the monkey during saccadic eye movements and fixation. J. Physiol. Lond. 300:539-555.

Katz B, Miledi R (1968) The role of calcium in neuromuscular facilitation. J Physiol (Lond) 434:183-213.

Kleinfeld D, Delaney KR (1996) Distributed Representation of Vibrissa Movement in the Upper Layers of Somatosensory Cortex Revealed with Voltage-Sensitive Dyes. J Comp. Neurology 375:89-108.

Kocsis JD, Malenka RC, Waxman SG (1983) Effects of extracellular potassium concentration on the excitability of the parallel fibres of the rat cerebellum. J Physiol. 334:225-44.

Konnerth A, Obaid AL, Salzberg BM (1987) Optical recording of electrical activity from parallel fibers and other cell types in skate cerebellar slices in vitro. J. Physiol. 393:681-702

Kues WA, Wunder F (1992) Heterogeneous expression patterns of mammalian potassium channel genes in developing and adult rat brain. European Journal of Neuroscience 4:1296-1308

Kuhn B (2001) Messungen von Aktionspotentialen in Dendriten von kultivierten und gentechnisch veränderten Hippocampusneuronen mit spannungssensitiven Farbstoffen. Dissertation, Technische Universität München.

Li W, Kaczmarek LK, Perney TM. (2001) Localization of two high-threshold potassium channel subunits in the rat central auditory system. J Comp Neurol 437(2):196-218.

Linden DJ, Dickinson MH, Smeyne M, Connor JA (1991) A long-term depression of AMPA currents in cultured cerebellar Purkinje neurons. Neuron 7:81-89

Lu C, Mattson MP (2001) Dimethyl Sulfoxide Suppresses NMDA- and AMPA-Induced Ion Currents and Calcium Influx and Protects against Excitotoxic Death in Hippocampal Neurons. Experimental Neurobiology 170:180-185.

Macica CM, Kaczmarek LK (2001) Casein Kinase Determines the Voltage Dependence of the Kv3.1 Channel in Auditory Neurons and Transfected Cells J Neurosci 21(4):1160-1168.

Magleby KL (1987) Short-term changes in synaptic efficiency. In: Synaptic function (Edelman GM, Gall WE, Cowan WM, eds), pp 21-56. Wiley, New York.

Malenka RC, Kocsis JD, Ransom BR, Waxman SG (1981) Modulation of Parallel Fiber Excitability by Postsynaptically Mediated Changes in Extracellular Potassium. Science 214:339-341.

Malenka RC, Kocsis JD (1982) Effects of GABA on Stimulus-Evoked Changes in $[K^+]_0$ and Parallel Fiber Excitability. J Neurophysiology 48(3):608-621.

Malenka RC, Kocsis JD, Waxman SG (1983) The supernormal period of the cerebellar parallel fibers effects of [Ca2+]o and [K+]o. Pflugers Arch. 397(3):176-83.

Manabe T, Wyllie DJ, Perkel DJ, Nicoll RA. (1993) Modulation of synaptic transmission and long-term potentiation: effects on paired pulse facilitation and EPSC variance in the CA1 region of the hippocampus. J Neurophysiol 70(4):1451-1459.

Marr D (1969) A theory of cerebellar cortex. J Physiol. (Lond.) 202:437-470

Martina M, et. al. (1999) Functional and molecular differences between voltage.gated K^+ channels of fast-spiking interneurons and pyramidal neurons of rat hippocampus. J. Neurosci. 18:8111-8125.

Mateos JM, Benitez R, Elezgarai I, Azkue JJ, Lazaro E, Osorio A, Bilbao A, Donate F, Sarria R, Conquet F, Ferraguti F, Kuhn R, Knöpfel T, Grandes P (2000) Immunolocalization of the mGluR1 b splice variant of the metabotropic glutamate receptor 1 at parallel fiber – Purkinje cell synapses in the rat cerebellar cortex. J. Neurochem. 74:1301-1309

Matsukawa H, Wolf AM, Matsushita S, Joho RH, Knopfel T (2003) Motor dysfunction and altered synaptic transmission at the parallel fiber-Purkinje cell synapse in mice lacking potassium channels Kv3.1 and Kv3.3. Journal of Neuroscience 23(20):7677-84.

Matthews G (1996) Neurotransmitter release. Ann. Rev. Neurosci. 18:219-233.

Migliore M, Morse TM, Davidson AP, Marenco L, Shepard GM, Hines ML (2002) ModelDB: making models publicly accessible to support computational neuroscience. Neuroinformatics 1:135-140

Monyer H, Burnashev N, Laurie DJ, Sakmann B, Seeburg PH (1994) Developmental and regional expression in the rat brain and functional properties of four NMDA receptors. Neuron 12:529-540.

Moreno H, Vega-Saenz de Miera E, Nadal MS, Amarillo Y, Ruby B (2001) Modulation of Kv3 potassium channels expressed in CHO cells by a nitric oxide-activated phoshatase. J Physiol. 530(3):345-358.

Mugnaini E, Floris A (1994) The unipolar brush cell: a neglected neuron of the mammalian cerebellar cortex. J Comp Neurol. 339(2):174-80.

Nakahiro M, Arakawa O, Narahashi T, Ukai S, Kato Y, Nishinuma K, Nishinuma T (1992) Dimethyl sulfoxide (DMSO) blocks GABA-induced current in rat dorsal root ganglion neurons. Neuroscience Letters 138:5-8.

Nicholson C, Steinberg R, Stöckle H, Ten Bruggencate G (1976) Calcium decrease associated with aminopyridine-induced potassium increase in cat cerebellum. Neuroscience Letters 3:315-319.

Nicholson C, Ten Bruggencate G, Steinberg R, Stöckle H (1977) Calcium modulation in brain extracellular microenvironment demonstrated with ion-selective micropipette. Proc. Nat. Acad. Sci. 74(3):1287-1290.

Nicholson C, Ten Bruggencate G, Stöckle H, Steinberg R (1978) Calcium and Potassium Changes in Extracellular Microenvironment of Cat Cerebellar Cortex. J. Neurophysiol. 41(4):1026-1039.

Ozaita A, Martone ME, Ellisman MH, Rudy B (2002) Differential Subcellular location of the Two Alternatively Spliced Isoforms of the Kv3.1 Potassium Channel Subunit in Brain. J. Neurophysiol. 88:394-408.

Palay S, Chan-Palay V (1974) Cerebellar Cortex. Springer Verlag, Berlin.

Pekhletski R, Gerlai R, Overstreet LS, Huang X, Agopyan N, Slater NT, Abramow-Newerly W, Roder JC, Hampson DR (1996) Impaired Cerebellar Synaptic Plasticity and Motor Performance in Mice lacking the mGluR4 Subtype of Metabotropic Glutamate Receptor. J Neurosci. 16(20):6364-6373.

Petralia RS, Wang YX, Singh S, Wu C, Shi L, Wei J, Wenthold RJ (1997) A monoclonal antibody shows discrete cellular and subcellular localization of mGluR1 alpha metabotropic glutamate receptors. J. Chem. Neuroanat. 13:77-93.

Porcello DM, Ho CS, Joho RH, Huguenard JR (2002) Resilient RTN Fast Spiking in Kv3.1 Null Mice Suggests Redundancy in the Action Potential Repolarization Mechanism. J Neurophysiol 87(3):1303-10.

Rall W (1995) The Theoretical Foundation of Dendritic Function. Selected Papers of Wilfried Rall with Commentaries. MIT Press, Cambridge, 1995.

Ravin R, Spira ME, Parnas H, Parnas I (1997) Simultaneous measurement of intracellular Ca^{2+} and asynchroneous transmitter release from the same crayfish bouton. J. Physiol. 501(2):251-262.

Regehr WG, Atluri PP (1995) Calcium transients in cerebellar granule cell presynaptic terminals. Biophys. J. 68:2156-2170

Reinert K, Dunbar RL, Chen G, Gao W, Ebner TJ (2002) New Intrinsic Signal in the Cerebellar Cortex. *2002 Abstract Viewer/Itinerary Planner.* Washington, DC: Society for Neuroscience.

Roberts WM, Jacobs RA, Hudspeth AJ (1990) Colocalization of ion channels involved in frequency selectivity and synaptic transmission at presynaptic zones of hair cells. J. Neurosci. 10:3664-3684

Rudy B, Chow A, Lau D, Amarillo Y, Ozaita A, Saganich M, Moreno H, Nadal MS, Hernandez-Pineda R, Hernandez-Cruz A, Erisir A, Leonard C, Vega-Saenz de Miera E (1999) Contributions of Kv3 Channels to Neuronal Excitability. Ann. New York Acad. Sci. 868:304-343.

Rudy B, McBain CJ (2001) Kv3 channels: voltage-gated K+ channels designed for high-frequency repetitive firing. Trends Neurosci 24(9):517-26.

Sabatini BL, Regehr WG (1997) Control of neurotransmitter release by presynaptic waveform at the granule cell to Purkinje cell synapse. J Neurosci 17(10):3425-35.

Sabatini BL, Regehr WG (1999) Timing of synaptic transmission. Ann. Rev. Physiol. 61:521-542.

Sanchez JA, Ho CS, Vaughan DM, Garcia MC, Grange RW, Joho RH. (2000) Muscle and motor-skill dysfunction in a K^+ channel-deficient mouse are not due to altered muscle excitability or fiber type but depend on the genetic background. Pflugers Arch 440(1):34-41.

Sargent B (1992) Electrical Signaling, in Hall ZW (Ed.) An Introduction to Molecular Neuroscience. Sinauer Associates, Sunderland.

Sekirnjak C, Martone ME, Weiser M, Deerinck T, Bueno E, Rudy B, Ellisman M (1997) Subcellular localization of the K^+ channel subunit Kv3.1b in selected rat CNS neurons. Brain Research 766:173-187

Simon SM, Llinas RR (1985) Compartmentalization of the submembrane calcium activity during calcium influx and its significance in transmitter release. Biophys. J. 48:485-498.

Sultan F (2000) Exploring a critical parameter of timing in the mouse cerebellar microcircuitry: the parallel fiber diameter. Neuroscience Letters 280:41-44.

Tempia F, Miniaci MC, Anchisi D, Strata P. (1998) Postsynaptic current mediated by metabotropic glutamate receptors in cerebellar Purkinje cells. J Neurophysiol 80(2):520-8.

Tempia F, Alojado ME, Strata P, Knöpfel T (2001) Characterization of the mGluR(1)-mediated electrical and calcium signaling in Purkinje cells of mouse cerebellar slices. J Neurophysiol 86(3):1389-97.

Tominaga T, Tominaga Y, Yamada H, Matsumoto G, Ichikawa M (2000) Quantification of optical signals with electrophysiological signals in neural activities of di-4-ANEPPS stained rat hippocampal slices. J Neurosci Methods 102:11–23.

Tsutsui H, Wolf AM, Knopfel T, Oka Y (2001) Imaging postsynaptic activities of teleost thalamic neurons at single cell resolution using a voltage-sensitive dye. Neurosci Lett. 312(1):17-20.

Veh RW, Lichtinghagen R, Sewing S, Wunder F, Grumbach IM, Pongs O (1995) Immunohistochemical Localization of Five Members of the Kv1 Channel Subunits: Contrasting Locations and Neuron-specific Co-localizations in Rat Brain. European Journal of Neuroscience 7:2189-2205.

Vranesic I, Iijima T, Ichikawa M, Matsumoto G, Knöpfel T (1994) Signal transmission in the parallel fiber – Purkinje cell system visualized by high-resolution imaging. Proc. Nat. Acad. Sci. 91:13014-17.

Wang H, Kunkel DD, Schwartzkroin PA, Tempel BL (1994) Localization of Kv1.1 and Kv1.2, Two K Channel Proteins, to Synaptic Terminals, Somata and Dendrites in the Mouse Brain. J. Neurosci. 14(8):4588-4599.

Wang LY, Gan L, Forsythe ID, Kaczmarek LK (1998) Contribution of the Kv3.1 potassium channel to high-frequency firing in mouse auditory neurones. J Physiology 509:183-194.

Weiser M, Vega-Saenz de Miera E, Kentros C, Moreno H, Franzen L, Hillman D, Baker H, Rudy B (1994) Differential expression of Shaw-related K+ channels in the rat central nervous system. J Neurosci 14(3 Pt 1):949-72.

Welker W (1987) Spatial Organization of Somatosensory Projections to Granule Cell Cerebellar Cortex: Functional and Connectional Implications of the Fractured Somatotopy (Summary of Wisconsin Studies). New Concepts in Cerebellar Neurobiology, Alan R. Liss, pp. 239-280

Welker W (1992) Guide to the Anatomy of the Brain: Cerebellum. In: Encyclopedia of Learning and Memory. Squire LR (Ed.) Macmillan Publ. Comp., New York.

Winckler B, Forscher P, Mellman I (1999) A diffusion barrier maintains distribution of membrane proteins in polarized neurons. Nature 397:698-701.

Xu-Friedmann MA, Harris KM, Regehr WG (2001) Three-Dimensional Comparison of Ultrastructural Characteristics at Depressing and Facilitating Synapses onto Cerebellar Purkinje Cells. J Neurosci. 21(17):6666-6672.

Zucker RS (1989) Short-term synaptic plasticity. Ann. Rev. of Neuroscience 12:13-31.

Zucker RS (1999) Calcium- and activity-dependent synaptic plasticity. Curr. Opin. Neurobiology 9:305-313.

Zucker RS, Regehr WG (2002) Short-term synaptic plasticity. Ann. Rev. Physiol. 64:355-405.

Annex 1

Using electro-optic switching of the laser to avoid smear and increase the optical imaging time resolution.

Using a laser as a light opened up the possibility to change the illumination (excitation light) intensity with an electro-optic crystal and a polarizing beam splitter. The electro-optic crystal rotates the polarization of the laser beam depending on the voltage applied. In connection with the polarizing beamsplitter deflecting the horizontally polarized component, this allows extremely fast switching of the laser intensity. The components of the system can be seen in Figure 2.3.

The PixelVision FastOne camera uses split frame transfer architecture with 4 output channels. That means the camera will electronically transfer the image on the CCD to both sides of the chip, with 2 output AD converters located on both sides. If exposure continues during the frame transfer, so-called “smear” will appear in the image. An example of smear is shown in Figure A1.1. Turning off the illumination during frame transfer will abolish smear (not shown).

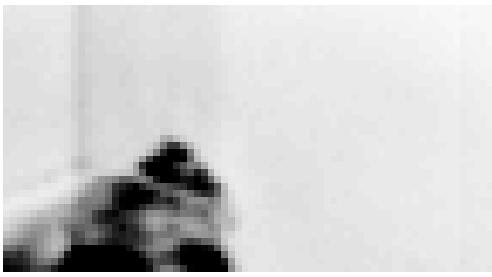

Fig. A1.1: Smear appearing in the FastOne camera in the presence of large contrast. To emphasize the smear (in vertical direction), the image was inverted and the tone curve adjusted.

Fast switching of the excitation light can not only abolish smear but also increase the time resolution of optical imaging. This works using the same

principle as stroboscopic imaging in photography. By restricting light exposure of the CCD by switching the excitation light using the electro-optic crystal, exposure times shorter than the limit imposed by the CCD can be realized. The resulting image series will contain data only from the time the excitation light was turned on. Additional acquisitions can then be used to obtain data from the remaining time. The acquisitions can then be combined to a single time series (movie) with increased time resolution (compared to conventional acquisition). The principle is outlined in Figure A1.2, where two acquisitions are used to double the time resolution.

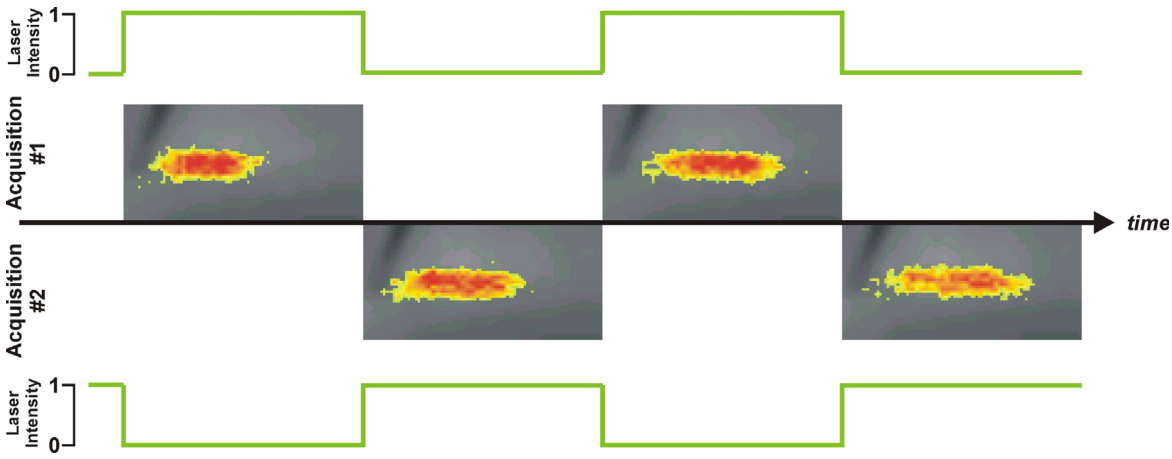

Fig. A1.2: Principle of stroboscopic illumination to increase time resolution. The example pictures are from 2 acquisitions shifted 200 microseconds relative to each other. The laser switching is sufficiently stable to result in movies of the same signal-to-noise ratio as from conventional acquisitions.

Limitations

First, this technique requires a laser as the light source, and lasers are currently not widespread light sources for optical imaging experiments of this kind, as they are usually quite noisy (random fluctuations in laser intensity). To increase the time resolution by a factor of 2, 2 acquisitions have to be used.

This increases not only the time necessary to obtain a single continuous data set, but makes it also necessary that the process observed does not change during acquisition. In this work, optical imaging data was usually the average of 16 repetitions of the same experiment and repeating the acquisition showed that the results did not change significantly during a single acquisitions. Nevertheless slow changes occur in the slice and acquisitions should be interleaved in the fashion of acquisition #1 – 1st repetition, acquisition #2 – 1st repetition, acquisition #1 – 2nd repetition, acquisition #2 – 2nd repetition, acquisition #1 – 3rd repetition, and so on. This will minimize artifacts from slow changes in the signal.

This technique was not used to obtain data in this work. Smear did not pose a problem, as the important quantity in experiments was change in fluorescence rather than absolute fluorescence and frame transfer time is quite small. Furthermore, the time resolution achieved using conventional, continuous excitation was sufficient to detect differences between the genotype. Using 2 acquisitions to obtain a single continuous data set would have doubled the duration of the experiments, significant thinking of the large number of conditions that a single slice was tested for. Nevertheless, the example in figure A1.2 proves that the technology is working. As the stability of lasers improves, more and more fluorescence imaging will be done with lasers as the light source and this technique might find widespread application.

Annex 2

Custom LabView application for the FastOne camera

To use the PixelVision FastOne camera system to acquire externally triggered movies and save them in the MiCAM format, two applications, “Monitor” and “Acquire”, were programmed. Both applications are written using the National Instruments LabView programming environment.

Before starting to use the programs, the computer and the camera have to be turned on. The applications also use a digital IO board to implement trigger input and give out control signals like, for example, to control the illumination shutter.

Monitor

Monitor is used to adjust the image area by moving the sample and/or the camera, to adjust the focus by raising or lowering the camera, and to adjust the fluorescence intensity by varying the illuminating laser intensity. “Monitor” continuously acquires single images at a rate of about 2 Hz with the same expose time as used later to acquire the movie.

A signal to control the shutter is given at the at the National Instruments CB-50LP digital IO board (next to the Pixelvision control box) at digital output line B0 (output 31 (TTL signal) and 32 (GND)). The shutter should open correctly if the controller is activated via Master8 with a TTL pulse of 5 ms delay and a duration of 20 ms.

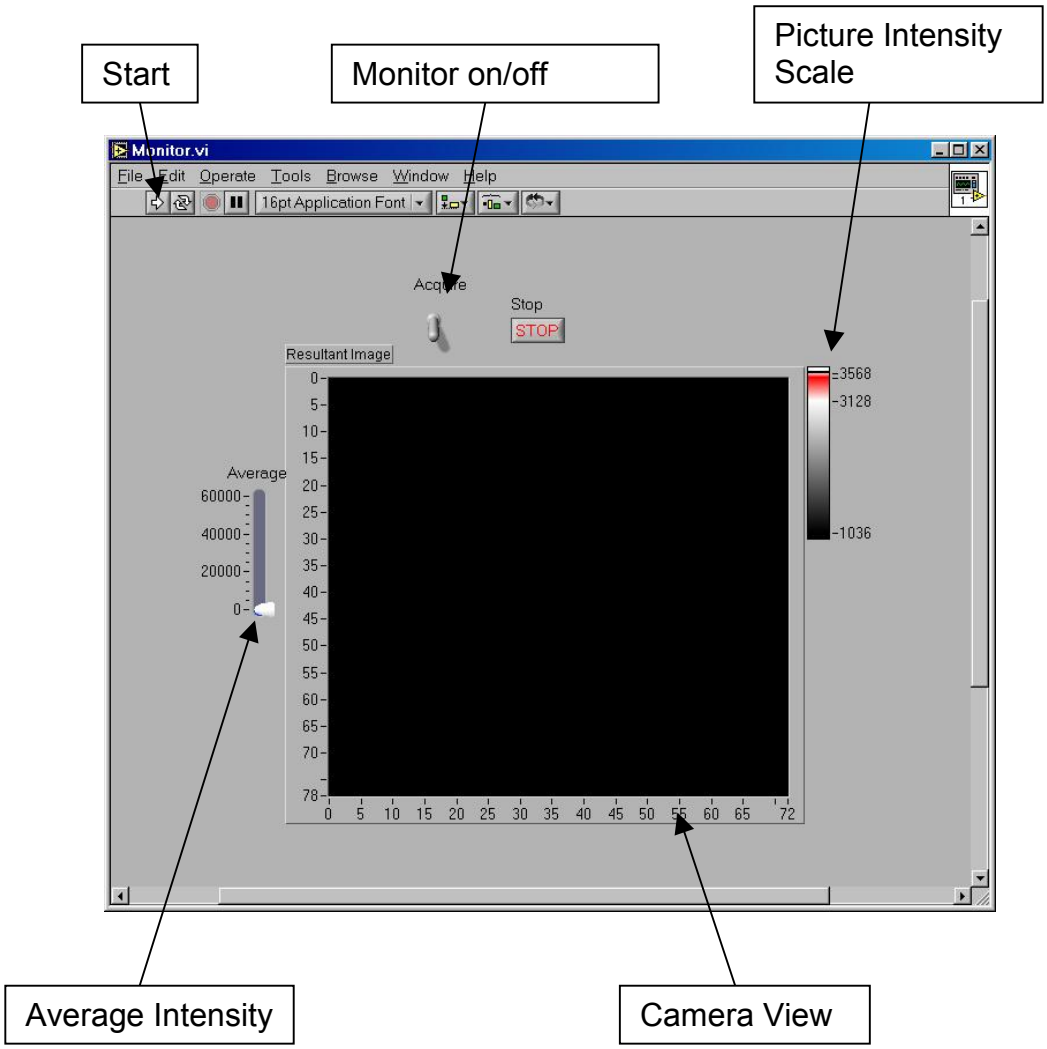

Fig. A2.1: *User interface of the "Monitor" application. Two scale bars are used to adjust the illumination intensity. The fixed scale "Average Intensity" displays average pixel intensity. The variable scale "Picture Intensity Scale" displays which pixel color in the central image corresponds to which pixel intesity. Both scales use the 12 bit range of the AD converter. Usually image intensity is adjusted so that red corresponds to slightly less than CCD full well capacity. Image acquisition can be turned on and off using the "Acquire" button.*

Acquire

“Acquire” is the application that permits starting the acquisition of movies using an external trigger. The resulting movie is stored in the BrainVision MiCAM file format.

“Acquire” records 682 frames (altogether lasting about 250ms) at a rate of 2.7kHz for a preselected number of times and saves the average in MiCAM file format (into “D:\FastOneData\”, which has to exist and provide enough free disk space). The filename will be “LVmmdd-hhmmss.dml” with mmdd being

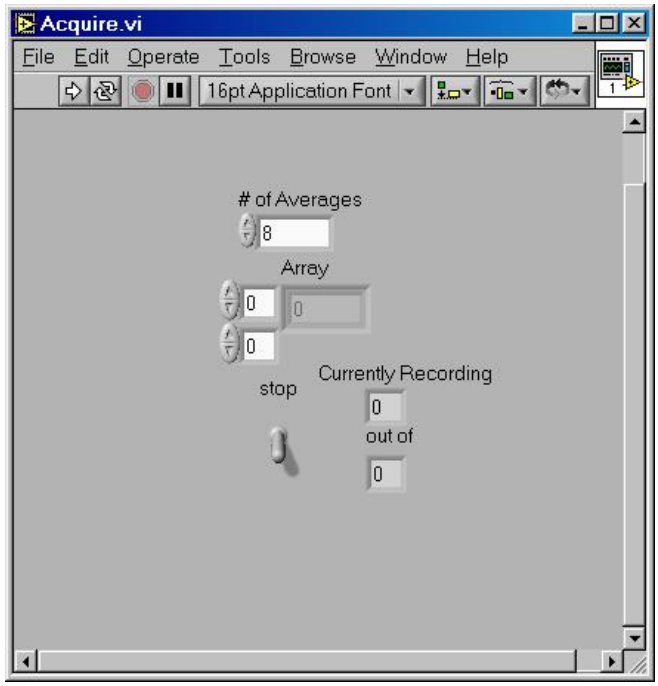

Fig. A2.2: User interface of the “Acquire” application. The number of acquisition to average can be adjusted in the uppermost field (usually 16). The array field allows one to navigate through the data, which can be used to check if the system is recording data correctly. Acquisition can be stopped using the “stop” button. The “Currently Recording” field displays which recording (out of the number of averages) is currently in progress.

the month and day of the month and hhmmss the time of saving the recording in hours, minutes and seconds. The suffix ".dml" is the MiCAM file format suffix.

Each acquisition is started when a TTL pulse (5V) arrives at the National Instruments CB-50LP digital IO board (next to the Pixelvision control box) at digital input line B1 (input 47 (TTL signal) and 48 (GND)), marked "Pixelvision Acquisition".

ANNEX 3

Purkinje cell anatomy in Kv3.1/3.3 double knockout mice

Motivation

Several mutant mice lacking cerebellar proteins exhibit changes in cerebellar anatomy. The unique anatomy of the Purkinje cell (PC) can not only be affected by the lack of key proteins, but also changes in the activity of the parallel fibers induce significant changes in PC anatomy (Bravin et al.,1999). It would not be surprising if changes in Parallel fiber – Purkinje cell transmission dynamics such as altered short-term plasticity and induction of metabotropic EPSCs with their assumed effect on plasticy affect one or more characteristics of Purkinje cell anatomy.

To investigate changes induced by the lack of Kv3.1 and Kv3.3 genes, Purkinje cell anatomy was compared between double knockout (DKO) and normal wild-type (WT) mice. This preliminary investigation with a small number of animals was done by immunostaining with fluorescent antibodies against the calcium-binding protein calbindin D-28k (Celio et al.,1990). Calbindin immunohistochemistry is routinely used to visualize Purkinje cell anatomy, since its expression in the cerebellar cortex is restricted to Purkinje cells (Garcia-Segura et al.,1984).

Methods

Animals were perfused transcardially with normal ACSF followed with 4% paraformaldehyde in 0.1 M phosphate buffered saline (PBS). The brain was removed from the skull and fixed at 4°C over night in 4% paraformaldehyde in PBS. The brain was then washed in PBS and the cerebellar cortex cut parasagittally in 50 µm sections. After repeated washing in PBS, the sections were blocked for 1 hour at room temperature in a solution containing 0.1 M PBS, 0.5% Triton-X and 5% fetal calf serum. The tissue was incubated with primary antibody at 4°C for 45 hours while gently shaking. The primary antibody solution was the blocking solution plus the primary antibody at a concentration of 1:1000 or 1:500. The slices were then washed 4 times 10 minutes in 0.1M PBS and incubated with the secondary antibody for 90 minutes at room temperature gently shaking. The secondary antibody solution was the blocking solution plus the secondary antibody at a concentration of 1:200. The slices were then washed 4 times 15 minutes in 0.1M PBS, once in 0.1 M phospate buffer and coverslipped.

The primary antibody was mouse anti-calbindind D-28K antibody (Swant, Bellizona, Switzerland). The secondary antibody was goat anti-mouse antibody conjugated to the Alexa 568 fluorophore (Molecular Probes).

Fluorescence images were obtained with an Olympus Fluoview upright laser scanning confocal microscope. Fluorescence was excited with a HeCd laser at 543nm wavelength. A 60X (N.A. 1.3) water immersion objective was used.

Results

The following images are from two 100 days old female DKO animals (Figures A3.1 & A3.2) and two 75 days old male WT mice (Figure A3.3 & A3.4), one picture from each animal.

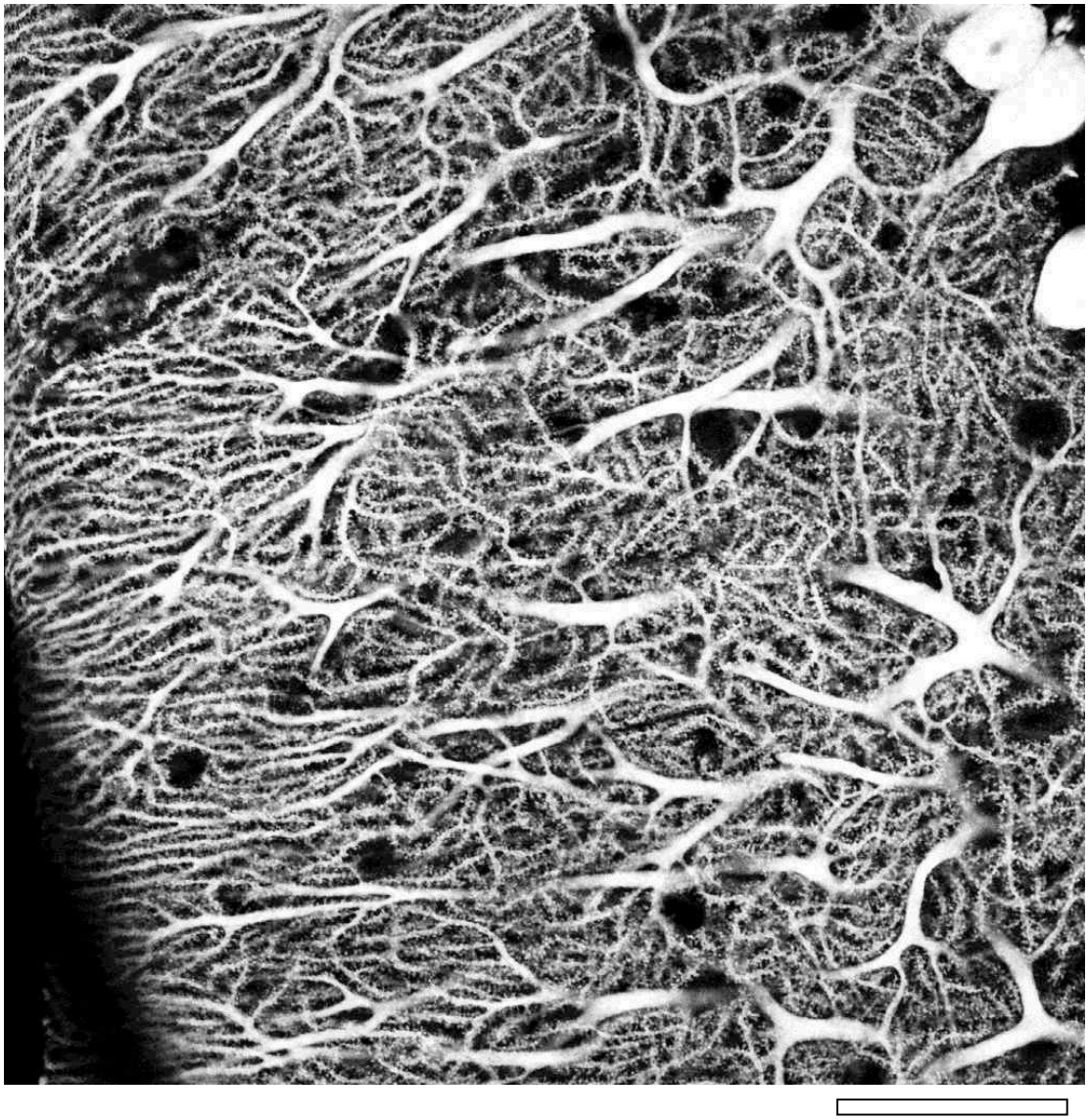

Fig.A3.1: DKO #1; confocal image of Purkinje cells stained with fluorescenct antibodies.The scale bar corresponds to 50 µm.

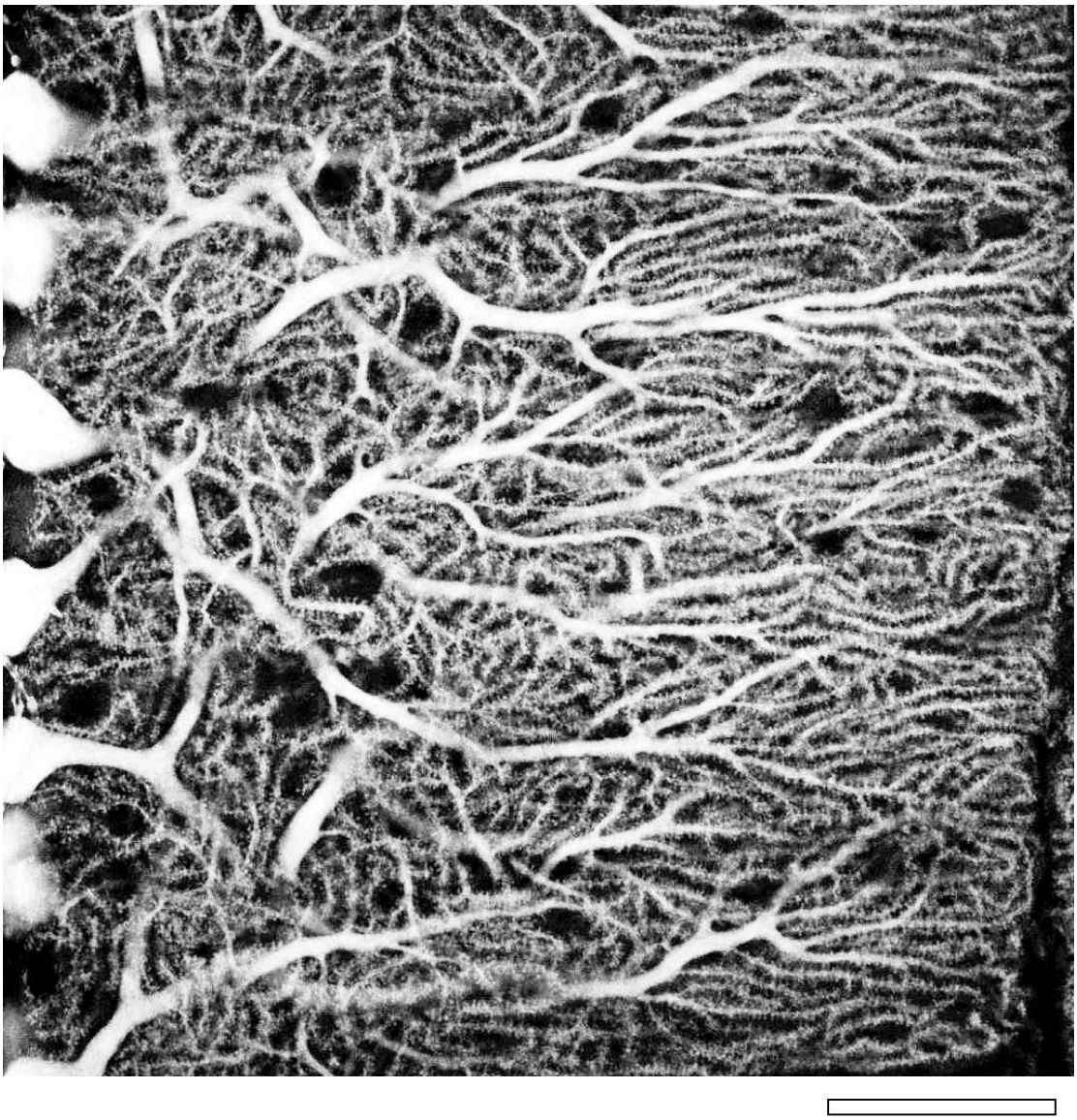

Fig.A3.2: DKO #2; confocal image of Purkinje cells stained with fluorescenct antibodies. The scale bar corresponds to 50 µm.

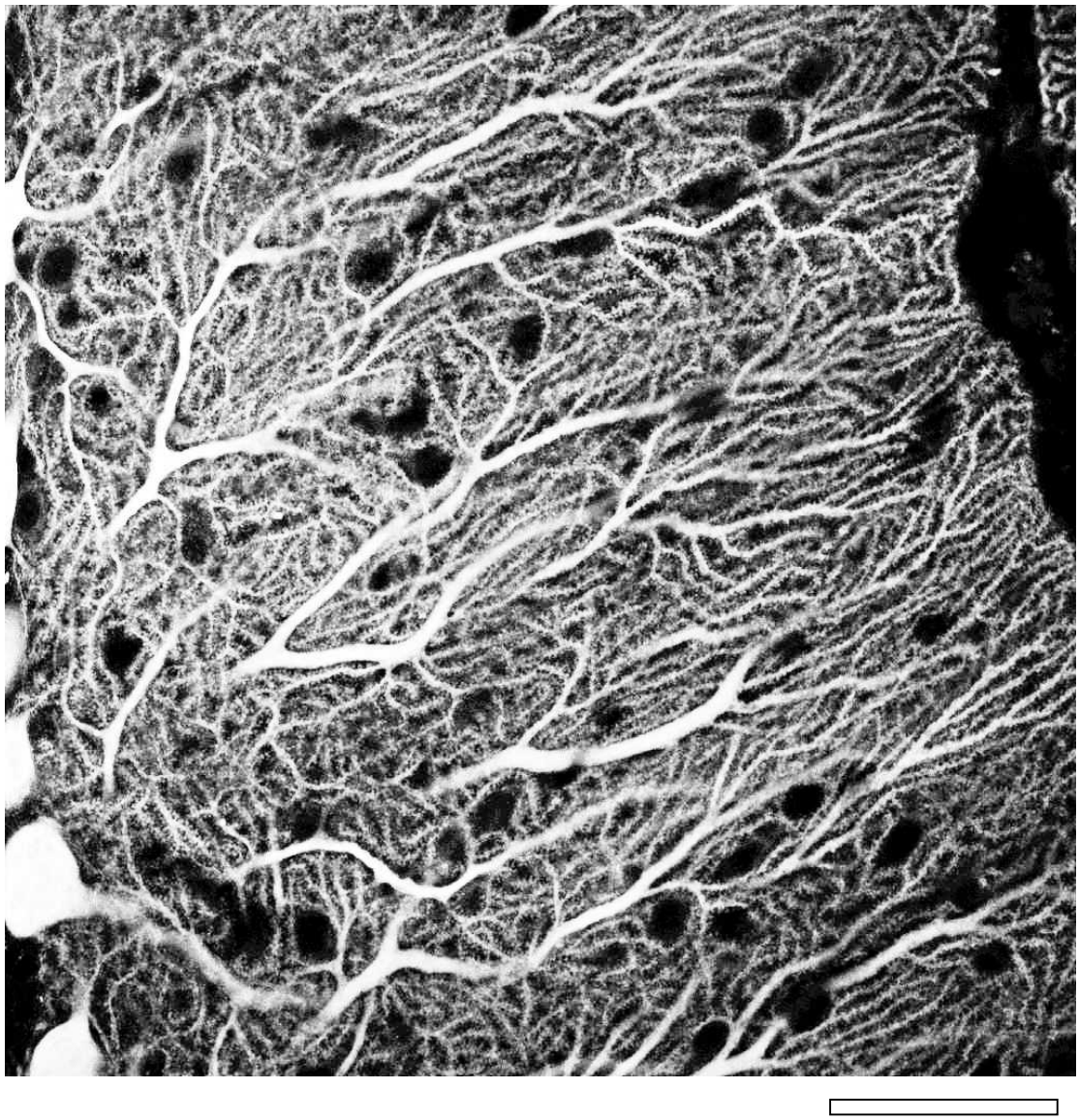

Fig.A3.3: WT #1; confocal image of Purkinje cells stained with fluorescenct antibodies. The scale bar corresponds to 50 µm.

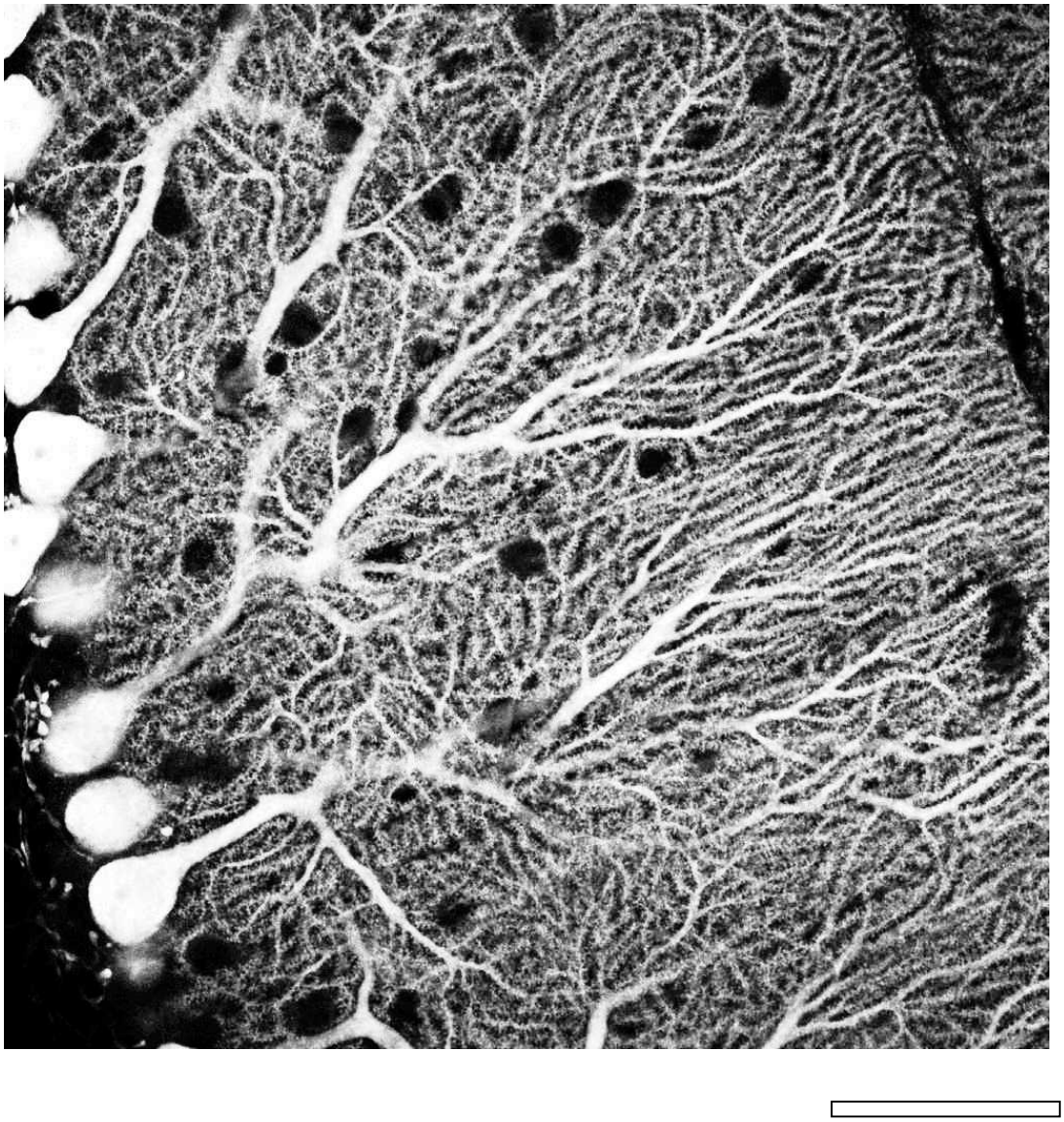

Fig.A3.4: WT #1; confocal image of Purkinje cells stained with fluorescenct antibodies. The scale bar corresponds to 50 µm.

Comparing the images, Purkinje cell primary dendrites seem to be thicker in DKO mice. The density of Purkinje cell dendrites also seems to be lower in the DKO animal. The density of dendritic spines seems to be unaffected at first sight. Two animals from each genotype are not enough to draw solid conclusion, so no attempt was made to quantify the apparent changes, but the

results suggest that Purkinje cell anatomy is also changed in the DKO. Since adult Purkinje cells express Kv3.3 (Rudy et al.,1999) and the channel is absent in DKO animals (a difference between DKO and WT in action potential afterhyperpolarization could be seen in patch clamp recordings from Purkinje cells), it can't be determined whether the apparent change is caused by the absence of Kv3 channels from Purkinje cells, the absence of Kv3.1 and Kv3.3 from parallel fibers, or a combination of the two.

Acknowledgement:

This work was supported by a grant of the RIKEN Brain Science Institute to Dr. Thomas Knopfel (G34-57625).

Thank you

Thank you to Dr. Thomas Knöpfel and the RIKEN Brain Science Institute for their support that made this work possible. To the japanese taxpayers for financing the excellent equipment. To Dr. Rolf Joho for providing and Shinichi Matsushita for breeding the Kv3 knockout mice. To Bibiana Scelfo and Walther Akemann for their help and advice. To Ayako Takada for her help. To Dr. Peter Fromherz, Dr. J. Leo van Hemmen and Dr. Filippo Tempia for supporting and reviewing this work. To the other members and former members of the Laboratory for Neuronal Circuit Dynamics at the RIKEN Brain Science Institute in Wako (Tokyo), Japan and the Department of Membrane and Neurophysics at the Max Planck Institute for Biochemistry in Martinsried (Munich), Germany for the warm atmosphere.
And to everybody else who contributed to the success of this work.